Aus der Klinik für Psychiatrie und Psychotherapie
Klinik der Ludwig-Maximilians-Universität München
Vorstand: Prof. Dr. med. Peter Falkai

PsyCoP – a novel platform for deep behavioral phenotyping and its use for the characterization of high validity psychiatric mouse models

Dissertation
zum Erwerb des Doktorgrades der Naturwissenschaften
an der Medizinischen Fakultät der
Ludwig-Maximilians-Universität zu München

vorgelegt von
Marius Stephan
aus
Gunzenhausen

Jahr
2022

Mit Genehmigung der Medizinischen Fakultät
der Universität München

Betreuer:	Univ.-Prof. Dr. rer. nat. Moritz Rossner
Zweitgutachter:	PD Dr. rer. nat. Carsten T. Wotjak
Dekan:	Prof. Dr. med. Thomas Gudermann
Tag der mündlichen Prüfung:	15. März 2023

Affidavit

LMU LUDWIG-MAXIMILIANS-UNIVERSITÄT MÜNCHEN | Promotionsbüro Medizinische Fakultät | MMRS

Eidesstattliche Versicherung

Stephan, Marius

Name, Vorname

Ich erkläre hiermit an Eides statt, dass ich die vorliegende Dissertation mit dem Titel:

PsyCoP – a novel platform for deep behavioral phenotyping and its use for the characterization of high validity psychiatric mouse models

selbständig verfasst, mich außer der angegebenen keiner weiteren Hilfsmittel bedient und alle Erkenntnisse, die aus dem Schrifttum ganz oder annähernd übernommen sind, als solche kenntlich gemacht und nach ihrer Herkunft unter Bezeichnung der Fundstelle einzeln nachgewiesen habe.

Ich erkläre des Weiteren, dass die hier vorgelegte Dissertation nicht in gleicher oder in ähnlicher Form bei einer anderen Stelle zur Erlangung eines akademischen Grades eingereicht wurde.

München, 12.04.2023

Ort, Datum

gez. Marius Stephan

Unterschrift Doktorand

Inhaltsverzeichnis

Abkürzungsverzeichnis

ACC	anterior cingulate cortex
AUD	Alcohol Use Disorder
BD	Bipolar Disorder
Bhlhe 40	Basic helix-loop-helix family, member e40
Bhlhe 41	Basic helix-loop-helix family, member e41
CA1	Cornu ammonis subfield 1
Cry 1	Cryptochrome Circadian Regulator 1
Cry 2	Cryptochrome Circadian Regulator 2
DKO	Double knockout
ECM	Extracellular matrix
ESARE	Enhanced Synaptic Response Element
GWAS	Genome-wide association study
GxE	Gene by environment interaction
LTP	long-term potentiation
MDD	Major depressive disorder
mEPSC	miniature excitatory post-synaptic potential
mPFC	Medial prefrontal cortex
NKX6.2	NK6 Homeobox 2
Nrg1	Neuregulin 1
OLIG2	Oligodendrocyte transcription factor 2
OPC	Oligodendrocyte progenitor cells
PsyCoP	Platform for systematic behavioral and cognitive profiling
RDoC	Research Domain Criteria
S	SOX10-transduced
scRNAseq	single-cell RNA sequencing
SCZ	Schizophrenia
SD	Social defeat
sEPSC	spontaneous excitatory post-synaptic potential
SON	SOX10/OLIG2/NKX6.2 co-transduced
SOX10	SRY-related HMG-box, member 10
STP	short-term potentiation
TCF4	Transcription factor 4
vHIP	ventral hippocampus

Publikationsliste

Die Publikationen sind in chronologischer Reihenfolge aufgeführt und Erstautoren fett gedruckt:

Stephan, M., Volkmann, P. & Rossner, M. J. Assessing behavior and cognition in rodents, non-human primates, and humans: where are the limits of translation? *Dialogues Clin Neurosci* **21**, 249–259 (2019). (Paper III; Anhang)

Hühne, A., Volkmann, P., Stephan, M., Rossner, M. & Landgraf, D. An In-Depth Neurobehavioral Characterization Reveals Anxiety-like Traits, Impaired Habituation Behavior, and Restlessness in Male Cryptochrome-deficient Mice. Genes, Brain and Behavior **19**, e12661. (Paper I)

Volkmann, P., Stephan, M., Krackow, S., Jensen, N. & Rossner, M. J. PsyCoP - A Platform for Systematic Semi-Automated Behavioral and Cognitive Profiling Reveals Gene and Environment Dependent Impairments of Tcf4 Transgenic Mice Subjected to Social Defeat. *Front Behav Neurosci* **14**, 618180 (2020). (Paper II)

Hühne, A., Echtler L., Kling C., Stephan M., et al. Circadian gene × environment perturbations influence alcohol drinking in Cryptochrome-deficient mice. Addict Biol e13105 (2021) doi:10.1111/adb.13105. (Paper IV; Anhang)

Raabe, F. J., Stephan M. et al. Expression of Lineage Transcription Factors Identifies Differences in Transition States of Induced Human Oligodendrocyte Differentiation. Cells 11, 241 (2022). (Paper VII; Anhang)

Stephan M., Schoeller J. et al. Spironolactone alleviates schizophrenia-related reversal learning in Tcf4 transgenic mice subjected to social defeat. Schizophr 8, 1–13 (2022). (Paper V; Anhang)

1. Beitrag zu den Veröffentlichungen

1.1 Beitrag zu Paper I

Zweitautorenschaft. Mein Beitrag zur Studie umfasst die Etablierung der Protokolle zum automatisierten Kameratracking in Light-Dark-Box-Test. Das Protokoll zur Durchführung des Prepulse-Inhibition-Test wurde von mir im Labor in der verwendeten Form etabliert. Zudem erstellte ich die Erstanalyseprotokolle für den Prepulse-Inhibition-Test und den Social-Interaction-Test sowie alle IntelliCage-basierten Tests.

Darüber hinaus stammen die IntelliCage-Programme zum Progressive-Ratio-Test, Place-Preference-Test, Reversal-Learning-Test, Sucrose-Preference-Test und Impulsivity-Test von mir. Im Fall von Progressive Ratio handelt es sich um eine Erstumsetzung des Tests im IntelliCage. Die übrigen Tests wurden von zuvor publizierten IntelliCage-Experimenten inspiriert.

In allen IntelliCage-Experimenten analysierte ich alle Daten aus IntelliCage-Experimenten und konzipierte die Analyse für den Progressive-Ratio-Test und Impulsivity-Test von Grund auf neu.

Außerdem erstellte ich die detaillierte Analyse zur zirkadianen Aktivität inklusive der Abbildungen in Figure 1.

Zuletzt war ich am Schreiben und der Überarbeitung des Manuskripts beteiligt.

1.2 Beitrag zu Paper II

Geteilte Erstautorenschaft mit Paul Volkmann. Die Reihenfolge der Nennung der Erstautoren durch den Umfang des Beitrags zur Studie begründet. Die geteilte Erstautorenschaft wurde gewählt, da Paul Volkmann überwiegend für die Durchführung der Experimente und ich überwiegend für die Analyse verantwortlich war. So ergab sich ein gleich großer Beitrag zur Studie.

Im Detail umfasste mein Beitrag den Test und die Auswahl der Experimente, ich war federführend bei der Konzipierung der Analysebatterie und insbesondere der Implementierung der IntelliCage-Experimente.

Darüber hinaus hatte ich den Großteil des Schreibens der FlowR-basierten Analysetoolbox übernommen, insbesondere stammte die Integration der Statistik und Dimensionsreduktionsanalyse sowie der Erstellung aller Diagramme aus meiner Hand, mit Ausnahme der Heatmap in Figure 5 welche von Paul Volkmann generiert wurde.

Ich unterrichtete Paul Volkmann in der Durchführung der Verhaltensexperimente. Zudem trug ich zur Durchführung der Verhaltensexperimente bei, sowohl zu Social-Defeat als auch den IntelliCage-Experimenten.

Das Schreiben und Überarbeiten des Manuskripts wurden von Paul Volkmann und mir zu gleichen Teilen übernommen.

1.3 Beitrag zu Paper III (Anhang)

Erstautorenschaft. Ich übernahm den überwiegenden Anteil der Konzipierung, Recherche und das Schreiben des Review-Artikels.

1.4 Beitrag zu Paper IV (Anhang)

Zweitautorenschaft. Für diese Publikation etablierte ich den Elevated-Plus-Maze-Test im Labor mit automatisiertem Kameratracking und Analyse. Bei den IntelliCage-Experimenten baute ich die für das Shift-Work-Experiment benötigten Dunkelboxen mit IntelliCage und Zeitschaltfuhren auf. Außerdem programmierte ich die dazugehörigen IntelliCage-Experimente und analysierte die Daten gezeigt in Figure 2, Figure 4 und Figure 5. Für Figure 5 A und B erstellte ich die dargestellten Graphen.

1.5 Beitrag zu Paper V (Anhang)

Geteilte Erstautorenschaft mit Jonathan Schoeller. Die Reihenfolge der Nennung der Erstautoren bedeutet keinen Unterschied im Umfang des Beitrags zur Studie. Die geteilte Erstautorenschaft wurde gewählt, da Jonathan Schoeller überwiegend für die Durchführung von Verhaltensexperimenten und ich überwiegend für die Analyse verantwortlich war. So ergab sich ein gleich großer Beitrag zur Studie.

Zu dieser Studie trug ich zur Konzipierung und dem Design bei. Darüber hinaus bildete ich Jonathan Schoeller in der Durchführung von Verhaltensexperimenten aus und unterstützte ihn bei deren Durchführung, insbesondere bei IntelliCage-Experimenten.

Zudem übernahm ich die Analyse aller erhobenen Daten mit Ausnahme der Gewichtsdaten, und erstellte die Statistik. Ich erstellte alle Abbildungen, mit Ausnahme von Figure 1A, die von Jonathan Schoeller erstellt wurde.

Bei der Erstellung des Manuskripts teilten sich Jonathan Schoeller und ich die anfallenden Aufgaben zu gleichen Teilen.

1.6 Beitrag zu Paper VI (Anhang, unpubliziert)

Erstautorenschaft. Das Manuskript ist zum Zeitpunkt der Abgabe dieser Arbeit noch nicht zur Publikation eingereicht.

Zu dieser Studie war ich in vollem Umfang verantwortlich für die Durchführung, Analyse und Darstellung der Verhaltensexperimente, des Einzelzell-RNA-Sequenzierungs-Experiments

(scRNAseq) und aller Experimente in primären, kortikalen Neuronen. Darüber hinaus wurden die statistischen Analysen und die Darstellungen der elektrophysiologischen Experimente von mir konzipiert und erstellt.

Alle Darstellungen in den Abbildungen Figure 2 bis Figure 4 sowie Figure S2 bis Figure S11 wurden von mir erstellt.

Die First-Draft-Version des Manuskripts wurde von mir verfasst und überarbeitet, mit Unterstützung von Sergi Papiol in den Kapiteln 3.1, 4.1 und 5 sowie von Weiqi Zhang und Mingyue Zhang in Kapitel 3.5.

1.7 Beitrag zum Paper VII (Anhang)

Zweitautorenschaft. In dieser Studie erstellte ich zuerst zusammen mit Florian Raabe ein Protokoll zur Vereinzelung von oligodendroglialen 2D-Kulturen. Des Weiteren führte ich die scRNAseq-Experimente durch und analysierte die gewonnenen Daten wie in der Sektion *2.7 Single-Cell RNA Sequencing and Data Analysis* des Artikels beschrieben. Darüber hinaus erstellte ich die Graphen in den Abbildungen Figure 3 bis Figure 6A – G sowie Figure S3 bis Figure S6.

Bei der Erstellung des Manuskripts war ich verantwortlich für die entsprechenden Kapitel, genauer 2.7 allein und 3.4 bis 3.8 in gleichwertiger Zusammenarbeit mit Florian Raabe. Auch zur Diskussion trug ich maßgeblich bei.

2. Introductory Summary (English)

2.1 Background

Translational psychiatric research has been in a crisis for several decades. The clinical need for new psychopharmacological medication is still very high. Treatment resistance and unaddressed symptoms are a huge burden on psychiatric disorder patients and society[1]. Nevertheless, decades of major investments in private and academic neuropharmacological research produced only minor returns most of the times. Drug development strategies that worked for cancer, immunology, and many other biomedical fields of research, failed to produce major improvements in psychiatry with high attrition rates[2].

This is, at least partially, a consequence of the genetic and phenotypic complexity of neuropsychiatric disorders. However, because of major technological progress with Genome-wide association studies (GWAS), the field is quickly progressing to understand the complex genetic architecture underlying polygenic psychiatric disorders such as, major depressive disorder (MDD)[3], schizophrenia (SCZ)[4] and bipolar disorder (BD)[5]. Moreover, the environment has major influence on neurodevelopment and in consequence on neuropsychiatric disease risk, adding to the complexity of pathogenesis and neuropathology. With environmental influences impacting disease risk as early as *in utero* development[6] and as late as adolescence[7], and environmental factors interacting with each other to produce a clinical phenotype[8], it is challenging to elucidate the interplay of genetics and environment.

Furthermore, the early neurodevelopmental aspects in the pathogenesis of neuropsychiatric disorders such BD[9] and SCZ[10,11] lead to irreversible changes in brain physiology and microanatomy, so that neuropharmacological treatment can only alleviate the consequences of these pathological changes and probably never “repair” the affected systems permanently. This often leads to misconceptions, assuming the mechanisms of pathogenesis ought to be similar to the mechanism of recovery, while they are very likely to be distinct.

Those mechanisms of recovery themselves are potentially as complex as the pathogenesis and etiologies. Elucidating all of these mechanisms, however, is of prime importance to understand treatment resistance, which is still a major issue in MDD, SCZ and BD alike.

In summary, our understanding of the neurobiology underlying psychiatric disorders is growing fast. Still, the development of neuropharmacological compounds is yet to pick up the pace of research progress. A major reason for this discrepancy is a lack of validated targets and high-validity models. Results from behavioral studies are often not reproducible or conflicting, and have low predictive value, possibly contributing to high attrition rates in clinical studies. In addition, there is a longstanding focus of neuropharmacological development on already known targets in the monoaminergic networks of the brain.

To improve the success of translational research in addressing the urgent clinical needs in psychiatry, we need improved models, incorporating the genetic nature of those disorders, such as patient-derived cellular models, and animal models reflecting the interaction of genetics and environment central to psychiatric disorder etiology. Further, animal research on psychiatric disorders needs to focus on conserved traits and endophenotypes, that are in some cases shared between psychiatric disorders. Moreover, we need to adopt new concepts incorporating the neurobiological basis of psychiatric disorders to guide research using those improved models. The field is quickly moving to meet these challenges. A detailed review on limits and future directions of translational psychiatry in animal models can be found in Stephan et al. (Paper III).

2.2 Aims

The primary aim of this thesis was to provide an innovative concept of behavioral endophenotyping thereby improving the analysis of psychiatric risk gene mouse models aiming to increase predictive value of preclinical treatment trials.

First, I developed an improved platform for systematic and semi-automated cognitive and behavioral profiling (PsyCoP) that represents a novel approach to the generation and analysis of comprehensive behavioral data. Second, we applied this platform, and extensions of it, to better characterize models for translational research on psychiatric disorders, i.e., the *Tcf4*-transgenic social defeat (*Tcf4x*SD) 'two-hit' model of cognitive deficits in schizophrenia (SCZ), the *Bhlhe40/41*$^{-/-}$ double-knockout (*Bhlhe40/41* DKO) mouse model of lithium non-responsiveness in bipolar disorder (BD), and the Cry1/2 double-knockout model of a reduced risk for alcohol use disorder (AUD). Third, we made use of state-of-the art single-cell transcriptomics to improve the characterization of a patient-derived cellular model of myelination that will be used in future studies to create the basis for an improved mouse model of disturbed myelination.

2.3 The concept behind PsyCoP - the standardized platform for systematic cognitive and behavioral profiling

With PsyCoP, we addressed several issues of translational animal studies in psychiatric research: First, we tried to improve on variability between runs in three ways: We automated both data acquisition and analysis wherever possible, reducing handling of the experiment mice to a minimum. A large portion of the experiments were automated using the IntelliCage system (TSE Systems GmbH, Germany). Further, we blinded the experimenter and reduced the risk of mix-ups in any stage of data analysis by identifying mice with the help of RFID chips, implanted before the actual experiments.

Second, we adopted the Research Domain Criteria (RDoC) concept[12]. The aim of RDoC is to provide a framework guiding translational research with a neurobiological basis. This takes form in the RDoC matrix, comprising neurobiological system domains and associated behav-

iors, tests, endophenotypes, cells, and other structures[13]. We used this matrix to group together informative variables assessed in PsyCoP's individual experiments in biologically meaningful domains, which are conserved between humans and mice.

Third, we analyzed the collected data as an overall neurocognitive profile rather than independent variables by using dimensional reduction analysis to generate a low-dimensional representation of phenotypic space. Furthermore, we fitted a multivariate linear model and corrected the statistical tests for multiple testing to gain statistically robust results.

2.4 Deep phenotyping of Cry1$^{-/-}$/Cry2$^{-/-}$ deficient mice with the PsyCoP prototype

One of the first models to be characterized in a PsyCoP prototype run was the Cry1$^{-/-}$/Cry2$^{-/-}$ double-knockout (Cry DKO) model described in Hühne et al. (Paper I). The Cry paralogs are modulators of the circadian clock[14] and circadian dysfunctions were associated with mood and anxiety disorders[15–18], making modulation of circadian clock functions a promising treatment option[19].

When we investigated the Cry DKO mouse model, the platform was not yet finished, so the article does not feature a PsyCoP style analysis and data presentation. However, most core PsyCoP experiments were conducted, revealing a prepulse inhibition deficit, as well as a reduction in novelty-induced but not general activity. In combination with an increased time immobile in the Light Dark Box experiment, this reduction in activity in a novel environment was interpreted as increased anxiety.

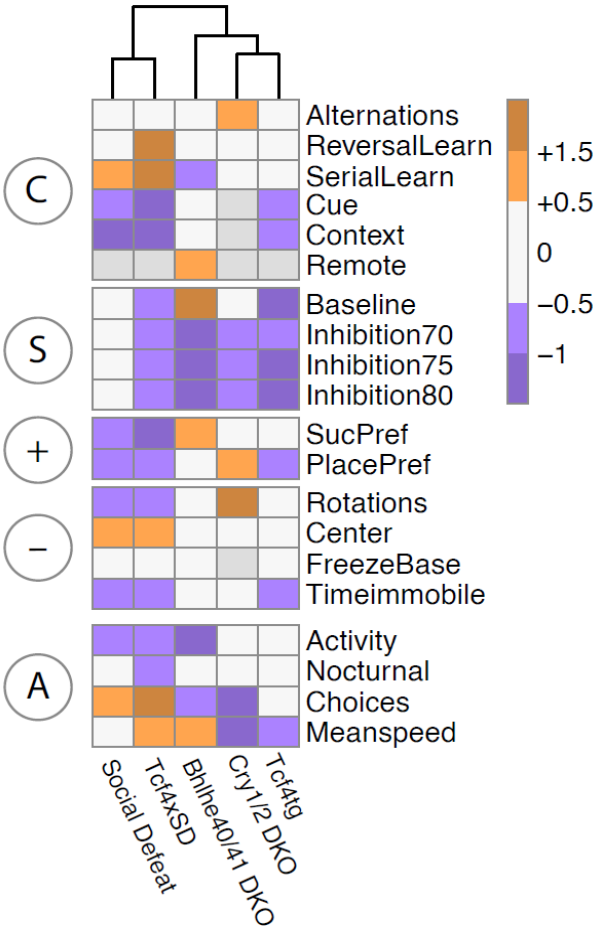

Figure 1. Z-score heatmap comparing mouse lines characterized with PsyCoP. Colors indicate Z-transformed difference in the respective measure between each mouse model to its wildtype reference. Orange panels represent positive differences (higher values), purple panels negative differences (lower values). Missing variables are shown as grey panels. In most variables a deviation in either direction can be assumed to be pathological. Variables are grouped according to RDoC domains: Cognitive (C), Sensorimotor (S), Positive (P) and Negative (N) Valence as well as Arousal and Regulatory (A) Systems domain. The dendrogram on top indicates unsupervised hierarchical clustering results (Manhattan distances).

When we compare the PsyCoP profile of Cry DKO mice to other mouse lines in a Z-score heatmap (Figure 1), they cluster with Bhlhe40/41 DKO and *Tcf4* transgenic mice driven mainly by the prepulse inhibition deficit. In contrast, psycho-social stress induced by social defeat is set apart from genetically induced behavioral disturbances in hierarchical clustering, mostly driven by severe cognitive impairments and a blunted positive valence system function.

Since circadian disturbances are considered a risk factor in AUD, we paired the Cry DKO genotype with a shift work paradigm in a follow-up study focused on alcohol drinking behavior, which was not compatible with the standardized phenotyping battery (Paper IV). In this study we found that shift work as a second hit exacerbates the alcohol consumption difference found in Cry DKO mice in a gene x environment (GxE) interaction.

2.5 *Tcf4*xSD – the first full PsyCoP profile

The first mouse model to be characterized with PsyCoP was the *Tcf4* transgenic social defeat (*Tcf4*xSD) 'two-hit' model (Paper II). In this pilot study we acquired a full neurocognitive

profile of a high face and structural validity mouse model of cognitive impairments in schizophrenia patients with the final streamlined experiment battery, allowing for a higher throughput in an academic laboratory setting.

In the *Tcf4*xSD model, we paired a mild genetic disturbance with an environmental influence, to study GxE interactions on behavioral level, improving over simple genetic mouse models still commonly used in translational psychiatric research.

For the genetic predisposition we chose a mildly increased expression of *Tcf4.* TCF4 is a pleiotropic psychiatric risk gene[20] and was recently demonstrated to be expressed higher in SCZ patients compared to healthy controls[11].

As previously mentioned, the environmental factor selected was psycho-social stress in adolescence, a late influence, commonly used in psychiatric research[21]. We found interactions in the cognitive systems domain, whereas negative and positive valence domains appeared to be influenced mainly by psychosocial stress and sensorimotor gating by the increase of *Tcf4* gene dosage. These findings did not only validate *Tcf4*xSD mice as a model of cognitive impairment in neuropsychiatric disorders, particularly schizophrenia, but also the validity of the *a priori* assignments of single variables to their RDoC domains. Of note, *TCF4* was also associated with bipolar disorder risk and the *Tcf4*xSD mouse likely is a high-validity model of cross-disorder cognitive endophenotypes rather than a model of cognitive symptoms in schizophrenia alone.

2.6 Treatment validation with the help of PsyCoP and the *Tcf4*xSD two-hit mouse model

In the next step, we used the *Tcf4*xSD model to validate the cognition improving effect of spironolactone (Paper V). Cognitive symptoms in SCZ patients are still not treated well by existing medication, creating a strong clinical need for new therapeutics addressing cognitive dysfunctions. Spironolactone, a previously discovered repurposed compound, had been shown to rescue working memory deficit in Neuregulin 1 transgenic (*Nrg1*tg) mice[22], making it a promising candidate for rescuing cognitive deficits found in SCZ by readjusting the skewed excitation/inhibition (E/I) balance the patient's cortex[23], which was also tested in a clinical trial, assessing cognitive performance of SCZ patients[24]. In our translational treatment study, we decided to test spironolactone not only alone but also in combination with aripiprazole, an atypical neuroleptic, since the positive symptoms of schizophrenia patients will be treated with a neuroleptic in a clinical context and drug interactions are a major concern. Moreover, we treated the mice orally while monitoring their drinking behavior and started testing only three weeks after treatment had started to avoid measuring acute drug effects, since in a clinical setting only chronic treatment will produce a favorable therapy outcome.

Most interestingly, we found that aripiprazole and spironolactone interfered with each other's effect on cognitive performance of *Tcf4*xSD mice, demonstrating the importance of testing new therapeutic candidates in a clinically relevant experiment design.

2.7 Modelling lithium treatment non-responsiveness by translating human genetics to a PsyCoP characterized mouse model

Another pressing clinical need arises from the fact that a majority of BD patients does not respond well to treatment with lithium, a widely applied mood stabilizer[25]. Moreover, lithium responsiveness is a heritable trait[26] and there is some research on the underlying genetics[25]. However, according to current knowledge, there is still no validated animal model for non-responsiveness, that will be instrumental when aiming at developing new therapies overcoming treatment resistance. Thus, the purpose of the study presented in Paper VI was to identify a genetic target for a high validity mouse model and to characterize this mouse model in a PsyCoP deep phenotyping approach.

In order to find potential candidates linked to lithium responsiveness, we conducted a gene-set-based association study on circadian genes and found an association of the core clock gene-set and lithium therapy outcome but not BD risk. This underlines that pathogenesis and recovery affect different mechanisms. Moreover, it shows that looking for affected systems via gene-set-based analyses might be powerful in identifying candidate genes following a global approach, under a polygenic background when single gene contributions are generally small.

In line, we identified *BHLHE41* as a major contributor to this association and selected it for further investigation. Next, I used PsyCoP to characterize the effect of chronic lithium treatment on *Bhlhe40/41* double knock-out (DKO) and wildtype control mice. In the PsyCoP profile, I found *Bhlhe40/41* DKO mice to be non-responsive to cognition enhancement by lithium treatment but still affected by its locomotor activity dampening effect. Moreover, I discovered a changed expression of post-synapse associated genes in *Bhlhe40/41* DKO anterior cingulate cortex layer 2/3 principal neurons, hinting to a change in synaptic plasticity. This was confirmed in primary cortical neuron cultures. Here, chronic lithium treatment dampened the response of a synapse-to-nucleus signaling sensor (ESARE) in wildtype cultures to stimulation. In contrast, *Bhlhe40/41* DKO cultures did not only show an already reduced level of excitability but were completely non-responsive to lithium treatment.

A reduced responsiveness was found on the level of electrophysiology in principal neurons in the layer 2/3 of the ACC and CA1 region of the ventral hippocampus (vHIP). In those cells, miniature and spontaneous excitatory postsynaptic currents (mEPSC; sEPSC) amplitudes were dampened after lithium treatment, but *Bhlhe40/41* DKOs were less responsive than wildtypes. An even stronger reduction in lithium responsiveness of *Bhlhe40/41* DKO excitatory neurons was found in LTP recordings in vHIP, linking the dampened excitability in response to lithium and the lowered response in *Bhlhe40/41* DKO mice directly to our observations on learning memory.

Although the underlying molecular mechanism still needs to be elucidated in future studies, *Bhlhe40/41* DKO mice are a promising candidate for a model of lithium non-responsiveness in BD patients, with an extensive neurocognitive PsyCoP profile for further use.

Moreover, the effect of BHLHE40/41 loss and gain of function on lithium responsiveness will be tested in patient-derived neuron cultures, closing the translational loop, and producing well-characterized and validated tools for future compound screens.

2.8 Oligodendroglia as a promising target for future animal studies

In another line of research, we approached the problem of target identification for model generation from a different angle by starting from patient-derived cell culture. These cultures carry the full genome of the donor patient and with it the full complexity of genetic pre-disposing factors. However, proper characterization of the differentiated cells is needed to allow for meaningful deductions from comparisons between patients and controls.

The cell lineage of interest in this project was oligodendroglia, since myelination was shown to be disturbed in MDD[27], SCZ[28], and BD patients[29]. Moreover, modulation of myelination is likely to be one of the major sources of plasticity in the adult brain, making it a promising target for treatment of these disorders[28]. In Paper VII, we employed scRNAseq with RNA velocity analysis to investigate the path and state of differentiation of human iPSCs driven by SOX10 alone (S) or in combination with OLIG2 and NKX6.2 (SON) and found that S cells tended to stay in an oligodendrocyte progenitor cell (OPC) stage, whereas SON cells differentiated to more mature oligodendrocytes. Moreover, we found that extracellular matrix (ECM) proteins were differentially expressed between S OPCs and more mature SON OPCs, hinting to an important role of ECM in the maturation of OPCs.

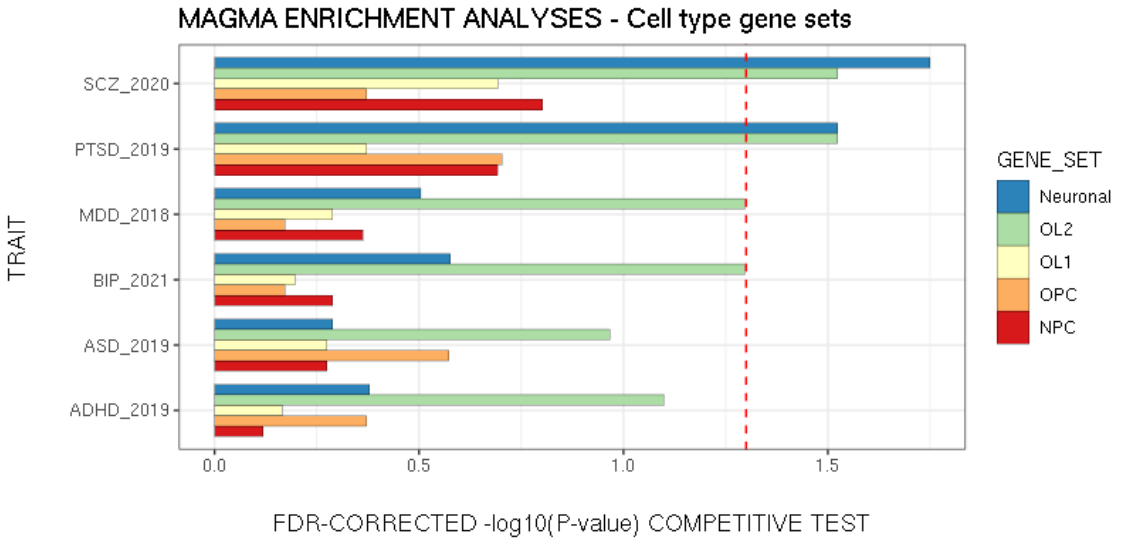

Figure 2. Expression profile of iOL2 cells is linked to life-time risk of several psychiatric disorders. MAGMA analyses based on expressed gene-sets of cell populations identified in S and SON cultures for the most recent psychiatric disorder risk GWAS data. Competitive test P-values in the X-axis are –log10 transformed. Dashed red line indicates the FDR corrected significance threshold P = 0.05. Created by Sergi Papiol. ASD: Autism spectrum disorder; ADHD: Attention deficit and hyperactivity disorder; BIP: Bipolar disorder

S and SON cultures will be used to compare SCZ patient-derived and healthy control-derived oligodendroglial cells in specific differentiation states, hopefully helping to elucidate, which oligodendroglial stages are affected in SCZ pathology. A first hint at the cell populations in those cultures with a high genetic risk load in their expression profile is shown in the MAGMA enrichment analysis (Figure 2). In this analysis, we could show an association of the transcriptome of the most mature oligodendrocyte population (iOL2) and the differentiation escaping immature neuronal cell population (Neuronal) with SCZ and post-traumatic stress disorder (PTSD) risk. Moreover, the OL2 transcriptome is significantly associated with MDD and BD risk, underlining the importance of oligodendrocytes for the pathogenesis of psychiatric disorders.

Future studies using SON cultures will hopefully identify promising gene candidates for a mutant mouse model. This genetic mouse model could be combined e.g., with social defeat, which has been shown to impact myelination in the mPFC of adult mice[30], to generate a high-validity two-hit model of disturbed myelination in SCZ. A PsyCoP profile of such a high construct validity mouse model will be a useful tool for compound validation screens and the elucidation of myelination mediated cognitive dysfunctions in SCZ.

3. Zusammenfassung

Es besteht nach wie vor dringender Bedarf an neuen psychopharmakologischen Medikamenten. Jedoch scheiterten bisher die meisten Entwicklungsversuche unter anderem aufgrund des Mangels an geeigneten und gut charakterisierten Zell- und Tiermodellen. In den letzten Jahren haben wissenschaftliche Fortschritte neue Einblicke in die Pathogenese von psychiatrischen Störungen und deren Heilung ermöglicht. Ziel dieser Arbeit war es, diese Fortschritte zu nutzen, um Targets zu identifizieren und Mausmodelle mit hoher Konstrukt-Validität zu charakterisieren. Dazu wurde ein neuartiger Ansatz zur Verhaltensprofilierung verwendet, um den prädiktiven Wert der Studien zu erhöhen.

Für eine tiefgreifende Phänotypisierung entwickelten wir eine standardisierte Plattform für die systematische und halbautomatische Erstellung von kognitiven und Verhaltensprofilen (PsyCoP) und untersuchten dabei das *Cry1/2*$^{-/-}$-Doppelknockout (*Cry*-DKO) -Mausmodell. Darüber hinaus haben wir den genetischen Faktor *Cry*-DKO mit einem Schichtarbeitssystem als Umweltfaktor kombiniert, um ein ätiologisch valides "Two-Hit"-Modell eines veränderten Risikos für Alkoholmissbrauchsstörungen (AUD) zu erhalten.

Des Weiteren habe ich eine Datenanalyse-Pipeline für PsyCoP entwickelt, die das *Research Domain Criteria* (RDoC)-Konzept für einen hohen translationalen Wert nutzt. Wir nutzten PsyCoP dann zunächst zur Charakterisierung des Tcf4-transgenen Modells gepaart mit psychosozialem Stress durch wiederholte soziale Niederlagen (*Social Defeat; Tcf4*xSD), um die Wechselwirkungen zwischen Genetik und Umgebung (GxE) zu untersuchen, die zu schweren kognitiven Störungen bei Schizophrenie und anderen psychotischen Störungen führen. Darüber hinaus validierten wir die positive Wirkung des kürzlich als pro-kognitiv wirkend identifizierten Wirkstoffs Spironolacton auf die kognitiven Funktionen im Tcf4xSD-Mausmodell.

Anschließend untersuchten wir die genetischen Grundlagen der Lithiumantwort mit Hilfe von Gen-Set-basierten *Enrichment*-Analysen und fanden einen starken Zusammenhang zwischen der zirkadianen Uhr und Lithiumtherapie-Erfolg. Darüber hinaus identifizierten wir den zirkadianen Modulator *BHLHE41* als einen Top-Hit. Anschließend wiesen wir nach, dass *Bhlhe40/41*$^{-/-}$-Doppelknockout-Mäuse (*Bhlhe40/41*-DKO) bei verschiedenen kognitiven Aufgaben teilweise nicht auf Lithium ansprechen. Diese verschlechterte Antwort fand sich auch für den Effekt von Lithium auf die neuronale Erregbarkeit und synaptische Plastizität. Diese Ergebnisse deuten darauf hin, dass die Modulation der neuronalen Erregbarkeit ein zentraler Mechanismus der therapeutischen Wirkung von Lithium sein könnte und *Bhlhe40/41*-DKO-Mäuse ein potenzielles Modell für Patienten sind, die nicht auf Lithium ansprechen.

Schließlich haben wir die Charakterisierung eines vom Patienten stammenden zellulären Modells der Myelinisierung mit Hilfe der RNA-Velocity-Analyse verbessert. Mit Hilfe dieser Modelle werden wir hoffentlich in der Lage sein, Targets für verbesserte Mausmodelle einer gestörten Myelinisierung zu identifizieren.

4. Abstract (English)

There is still an urgent clinical need for new psychopharmacological treatments due to this far unaddressed symptoms and treatment resistance. In the last decades most developments failed, also because of the lack of appropriate and well characterized cellular and animal models. In recent years, advances in human genetics and patient-derived cellular models fostered new insights in the pathogenesis of and recovery from psychiatric disorders. The aim of this thesis was to make use of these advances to identify targets and characterize high construct validity mouse models based on these targets, with the help of a novel approach to behavioral profiling and single-cell transcriptomics, to increase predictive value.

For deep phenotyping, we developed a standardized platform for systematic and semi-automated cognitive and behavioral profiling (PsyCoP), investigating the Cry1/2$^{-/-}$ double-knockout (Cry DKO) mouse model in the process. Further, we paired the Cry DKO genetic factor with a shift work paradigm as environmental factor to gain a high construct validity 'two-hit' model of a changed risk for alcohol use disorder (AUD).

In addition, I established an improved data analysis pipeline for PsyCoP, adopting the Research Domain Criteria (RDoC) framework for high translational value. We then used PsyCoP first to characterize the *Tcf4*-transgenic social defeat (*Tcf4x*SD) 'two-hit' model, revealing gene x environment (GxE) interactions producing severe cognitive dysfunctions found in schizophrenia and other psychotic disorders. Further, we validated the beneficial effect of the repurposed compound spironolactone on cognitive functions in the *Tcf4*xSD mouse model.

We went on to investigate the genetics underlying lithium responsiveness with gene-set-based enrichment analyses, finding a strong association of the circadian core clock and lithium therapy outcome. Further, we identified the circadian modulator BHLHE41 as a top hit. Then, we demonstrated partial lithium non-responsiveness of *Bhlhe40/41*$^{-/-}$ double-knockout (Bhlhe40/41 DKO) mice in several cognitive tasks. Further, we found reduced neuronal excitability and synaptic plasticity in response to lithium treatment, again, with a partial or total non-responsiveness of Bhlhe40/41 DKO mice. These findings suggest neuronal excitability modulation as a central mechanism of lithium's therapeutic effect and Bhlhe40/41 DKO mice as a potential model for non-responder patients.

Lastly, we improved the characterization of a patient-derived cellular model of myelination with the help of RNA velocity analysis. With the help of these models, we will hopefully be able to identify targets for improved mouse models of disturbed myelination.

In summary, we were able to characterize and use several high validity mouse models psychiatric disorder endophenotypes with the help of the PsyCoP that will hopefully help to improve the translational value preclinical animal study and thus the success of psychopharmacological development to meet psychiatric clinical needs.

5. Paper I

Titel: An In-Depth Neurobehavioral Characterization Reveals Anxiety-like Traits, Impaired Habituation Behavior, and Restlessness in Male Cryptochrome-deficient Mice

DOI-Direktlink: https://doi.org/10.1111/gbb.12661

6. Paper II

Titel: PsyCoP - A Platform for Systematic Semi-Automated Behavioral and Cognitive Profiling Reveals Gene and Environment Dependent Impairments of Tcf4 Transgenic Mice Subject-ed to Social Defeat

DOI-Direktlink: https://doi.org/10.3389/fnbeh.2020.618180

7. Literaturverzeichnis

1. GBD 2019 Diseases and Injuries Collaborators. Global burden of 369 diseases and injuries in 204 countries and territories, 1990-2019: a systematic analysis for the Global Burden of Disease Study 2019. *Lancet* **396**, 1204–1222 (2020).
2. Waring, M. J. *et al.* An analysis of the attrition of drug candidates from four major pharmaceutical companies. *Nat Rev Drug Discov* **14**, 475–486 (2015).
3. Amare, A. T. *et al.* Bivariate genome-wide association analyses of the broad depression phenotype combined with major depressive disorder, bipolar disorder or schizophrenia reveal eight novel genetic loci for depression. *Mol. Psychiatry* (2019) doi:10.1038/s41380-018-0336-6.
4. Consortium, T. S. W. G. of the P. G., Ripke, S., Walters, J. T. & O'Donovan, M. C. *Mapping genomic loci prioritises genes and implicates synaptic biology in schizophrenia*. 2020.09.12.20192922 https://www.medrxiv.org/content/10.1101/2020.09.12.20192922v1 (2020) doi:10.1101/2020.09.12.20192922.
5. Mullins, N. *et al.* Genome-wide association study of more than 40,000 bipolar disorder cases provides new insights into the underlying biology. *Nat Genet* **53**, 817–829 (2021).
6. Allswede, D. M. & Cannon, T. D. Prenatal inflammation and risk for schizophrenia: A role for immune proteins in neurodevelopment. *Dev. Psychopathol.* **30**, 1157–1178 (2018).
7. Krebs, M.-O., Kebir, O. & Jay, T. M. Exposure to cannabinoids can lead to persistent cognitive and psychiatric disorders. *European Journal of Pain* **23**, 1225–1233 (2019).
8. Dunn, A. L., Michie, P. T., Hodgson, D. M. & Harms, L. Adolescent cannabinoid exposure interacts with other risk factors in schizophrenia: A review of the evidence from animal models. *Neuroscience & Biobehavioral Reviews* **116**, 202–220 (2020).
9. Kloiber, S. *et al.* Neurodevelopmental pathways in bipolar disorder. *Neuroscience & Biobehavioral Reviews* **112**, 213–226 (2020).
10. Jaaro-Peled, H. & Sawa, A. Neurodevelopmental Factors in Schizophrenia. *Psychiatric Clinics of North America* **43**, 263–274 (2020).
11. Ruzicka, W. B. *et al. Single-cell dissection of schizophrenia reveals neurodevelopmental-synaptic axis and transcriptional resilience*. http://medrxiv.org/lookup/doi/10.1101/2020.11.06.20225342 (2020) doi:10.1101/2020.11.06.20225342.
12. Anderzhanova, E., Kirmeier, T. & Wotjak, C. T. Animal models in psychiatric research: The RDoC system as a new framework for endophenotype-oriented translational neuroscience. *Neurobiology of Stress* **7**, 47–56 (2017).
13. NIMH » RDoC Matrix. https://www.nimh.nih.gov/research/research-funded-by-nimh/rdoc/constructs/rdoc-matrix.shtml.
14. Michael, A. K., Fribourgh, J. L., Van Gelder, R. N. & Partch, C. L. Animal Cryptochromes: Divergent Roles in Light Perception, Circadian Timekeeping and Beyond. *Photochemistry and Photobiology* **93**, 128–140 (2017).
15. Germain, A. & Kupfer, D. J. Circadian rhythm disturbances in depression. *Hum Psychopharmacol* **23**, 571–585 (2008).

16. Landgraf, D. *et al.* Genetic Disruption of Circadian Rhythms in the Suprachiasmatic Nucleus Causes Helplessness, Behavioral Despair, and Anxiety-like Behavior in Mice. *Biol Psychiatry* **80**, 827–835 (2016).

17. Kalmbach, D. A., Pillai, V., Cheng, P., Arnedt, J. T. & Drake, C. L. Shift work disorder, depression, and anxiety in the transition to rotating shifts: the role of sleep reactivity. *Sleep Medicine* **16**, 1532–1538 (2015).

18. Roybal, K. *et al.* Mania-like behavior induced by disruption of CLOCK. *Proc Natl Acad Sci U S A* **104**, 6406–6411 (2007).

19. Hühne, A., Welsh, D. K. & Landgraf, D. Prospects for circadian treatment of mood disorders. *Ann Med* **50**, 637–654 (2018).

20. Calabrò, M. *et al.* Genetic variants associated with psychotic symptoms across psychiatric disorders. *Neurosci. Lett.* **720**, 134754 (2020).

21. Bartolomucci, A., Fuchs, E., Koolhaas, J. M. & Ohl, F. Acute and Chronic Social Defeat: Stress Protocols and Behavioral Testing. in *Mood and Anxiety Related Phenotypes in Mice* (ed. Gould, T. D.) 261–275 (Humana Press, 2009).

22. Wehr, M. C. *et al.* Spironolactone is an antagonist of NRG1-ERBB4 signaling and schizophrenia-relevant endophenotypes in mice. *EMBO Mol Med* **9**, 1448–1462 (2017).

23. Liu, Y. *et al.* A Selective Review of the Excitatory-Inhibitory Imbalance in Schizophrenia: Underlying Biology, Genetics, Microcircuits, and Symptoms. *Front Cell Dev Biol* **9**, 664535 (2021).

24. Hasan, A. *et al.* Add-on spironolactone as antagonist of the NRG1-ERBB4 signaling pathway for the treatment of schizophrenia: Study design and methodology of a multicenter randomized, placebo-controlled trial. *Contemp Clin Trials Commun* **17**, 100537 (2020).

25. Papiol, S., Schulze, T. G. & Alda, M. Genetics of Lithium Response in Bipolar Disorder. *Pharmacopsychiatry* **51**, 206–211 (2018).

26. Grof, P. *et al.* Is response to prophylactic lithium a familial trait? *J Clin Psychiatry* **63**, 942–947 (2002).

27. Sacchet, M. D. & Gotlib, I. H. Myelination of the brain in Major Depressive Disorder: An in vivo quantitative magnetic resonance imaging study. *Sci Rep* **7**, 2200 (2017).

28. Raabe, F. J. *et al.* Oligodendrocytes as A New Therapeutic Target in Schizophrenia: From Histopathological Findings to Neuron-Oligodendrocyte Interaction. *Cells* **8**, 1496 (2019).

29. Sehmbi, M. *et al.* Age-related deficits in intracortical myelination in young adults with bipolar disorder type I. *Journal of Psychiatry and Neuroscience* **44**, 79–88 (2019).

30. Lehmann, M. L., Weigel, T. K., Elkahloun, A. G. & Herkenham, M. Chronic social defeat reduces myelination in the mouse medial prefrontal cortex. *Sci Rep* **7**, 46548 (2017).

Anhang A: Paper III

Titel: Assessing behavior and cognition in rodents, nonhuman primates, and humans: where are the limits of translation?

DOI-Direktlink: https://doi.org/10.31887/DCNS.2019.21.3/mrossner

Anhang B: Paper IV

Titel: Circadian gene × environment perturbations influence alcohol drinking in Cryptochrome-deficient mice

DOI-Direktlink: https://doi.org/10.1111/adb.13105

Anhang C: Paper V

Titel: Spironolactone alleviates schizophrenia-related reversal learning in Tcf4 transgenic mice subjected to social defeat

DOI-Direktlink: https://doi.org/10.1038/s41537-022-00290-4

Anhang D: Manuskript zu Paper VI

Modulation of Neuronal Excitability and Plasticity by BHLHE41 Conveys Lithium Non-Responsiveness

Marius Stephan[1,2], Sergi Papiol[1,3,4], Mingyue Zhang[5], Niels Jensen[1], Eva Schulte[3], Peter Falkai[1], Thomas Schulze[3,6,7,8], Weiqi Zhang[5], Moritz J. Rossner[1]

[1]Department of Psychiatry and Psychotherapy, Laboratory of Molecular Neurobiology, University Hospital, LMU Munich, Germany

[2]International Max Planck Research School for Translational Psychiatry (IMPRS-TP), Munich, Germany

[3]Institute of Psychiatric Phenomics and Genomics (IPPG), University Hospital, LMU Munich, Germany

[4]Instituto de Salud Carlos III, Biomedical Network Research Centre on Mental Health (CIBERSAM), Barcelona, Spain

[5]Laboratory of Molecular Psychiatry, Department of Psychiatry, University of Muenster, Germany

[6]Intramural Research Program, National Institute of Mental Health, National Institutes of Health, U.S. Department of Health & Human Services, Bethesda, MD, USA

[7]Department of Psychiatry and Behavioral Sciences, Johns Hopkins University, Baltimore, MD, United States

[8]Department of Genetic Epidemiology in Psychiatry, Central Institute of Mental Health, Medical Faculty Mannheim, University of Heidelberg, Mannheim, Germany

Correspondence:

Moritz Rossner

Moritz.Rossner@med.uni-muenchen.de

Abstract

Most bipolar disorder (BD) patients are non-responsive to the first line mood stabilizer lithium. The mechanisms underlying lithium (non-)responsiveness are largely unknown, although recent evidence implicates neuronal excitability as critical component. Circadian dysfunctions have been strongly associated with BD and control of circadian excitability is a central feature of the molecular clock.

We tested the hypothesis that molecular clock components are modifiers of lithium (non-) responsiveness by using two enrichment analysis methods on the most recent GWAS data. We found that core clock gene sets are significantly associated with lithium response, but not with psychiatric disorders including BD. Among the top hits was BHLHE41, a modulator of the clock and homeostatic sleep.

Since BHLHE41 and its paralog BHLHE40 are functionally redundant, we assessed lithium response in double-knockout mutants (DKO). We demonstrated that DKOs are non-responsive to lithium's beneficial effect in various cognitive tasks. Single-cell RNA sequencing from medial prefrontal cortex identified a deregulated postsynapse-associated gene set in DKO excitatory neurons. Cellular assays and electrophysiological recordings revealed lowered levels of neuronal

excitability and plasticity mediated by lithium, and reduced lithium responsiveness of DKOs compared to wildtype mice.

Our findings suggest that lithium acts via modulation of neuronal excitability and synaptic plasticity depending on modulators of the molecular clock, including BHLHE41.

Introduction

Bipolar Disorder (BD) is one of the top disorders in global prevalence and disease burden[1]. Moreover, BD patients have a 20 to 30-fold increased suicide rate with an estimated 40 % heritability of completed suicide[2]. Symptomatically, BD is primarily a mood disorder characterized by, commonly recurrent, episodes of mania and, in case of BD Type II, depression.

First line medication for prophylaxis of episodes and reduction of suicidality is lithium in the form of its salts[3]. Lithium is unique among neuropharmacological compounds as a simple alkaline metal ion as well as for its long and rich history in the treatment neuropsychiatric conditions.

Lithium interacts with numerous proteins, making the distinction between therapy-relevant and side or even toxic effects difficult[4]. Elucidating lithium's mode of action is of particular interest because of a major unmet clinical need: Only about 30 % of BD patients are considered excellent responders, while remaining patients show only partial to no response to lithium treatment[5]. Additionally, lithium has a variety of adverse side effects, particularly nephrotoxicity, which often necessitates treatment breaks or ceasing treatment altogether, despite an excellent response[6]. Lithium responsiveness can also drop over time and in a few cases even discontinuation of lithium therapy after long-term use was found to compromise its effectiveness after resuming therapy[7].

A deeper understanding of the therapeutic mechanism of lithium and elucidation of the mechanism of lithium therapy non-responsiveness might lead to new treatments with the beneficial properties of lithium, but higher efficacy in resistant patients and more favorable side effect profiles.

In the past, many researchers have linked new findings on BD pathogenesis to mechanisms of lithium response and vice versa, assuming a largely overlapping genetic and neurophysiological basis[8–10]. Similar strategies were successful in providing useful insights into many human diseases, such as the dopamine hypothesis of schizophrenia. However, although there is undeniably a mechanistic link between pathophysiology and recovery, the distinction between trait and state is key in the treatment of psychiatric disorders as the neurodevelopmental pathogenesis might not be reversible[11]. Therefore, effective therapies might have to rely on the modulation of the neuronal function and plasticity that is still present in the adult brain.

Along these lines, lithium's effect on neuronal excitability and especially its neuroprotective properties were extensively studied in the past. Interestingly, lithium was found to increase excitability after acute treatment *in vitro*[12], but protects cortical neurons in culture from glutamate induced excitotoxicity at therapeutic serum concentrations, with effectiveness over time[13]. A similar discrepancy between acute and long-term effect was found for glutamate-reuptake at the pre-synapse[14] and modulation of adenylate cyclase activity[15]. Lithium therapy effects on mood

and suicidality depend on chronic treatment[16], therefore acute effects cannot be the cause of therapeutic actions. Thus, the delayed excitability and cAMP-signaling dampening effects might indicate that these mechanisms are involved in the actual therapeutic action. However, the most compelling evidence for its role in lithium's therapeutic effect is that the activity-dampening effect was demonstrated to be specific to patient-derived neuronal cultures from lithium responders and was not observed in cultures derived from lithium non-responder patients[17]. This finding suggests that lithium non-responsiveness is likely to be neuron autonomous, similar to lithium's neuroprotective and activity-dampening effect. In addition, it clearly demonstrates a genetic basis of lithium responsiveness. This is supported by studies showing lithium (non-)responsiveness is a familial trait[18], so we can assume that there is not only a major contribution of genetics to BD risk but also to (non-)responsiveness to lithium treatment and that the genetic architecture of BD risk and lithium responsiveness is likely to overlap.

One apparent convergence between BD endophenotypes and lithium response is the circadian molecular clock: BD patients were reported to exhibit abnormalities in circadian rhythms, with alterations in the sleep/wake cycle during manic and depressive phases and sleep problems during stable mood phases (euthymia)[19–21]. Likewise, alterations in body temperature, circadian cortisol rhythms, and melatonin levels have been reported in BD[22,23]. These disturbances have even been associated with increased relapse risk[24], poor metabolic health[25], and suicidality[26]. Moreover, mouse models for modulators of the circadian clock genes exhibit mixed-state endophenotypes of BD[27–29]. Circadian abnormalities might therefore represent a core biological susceptibility directly connected to hallmark symptoms of this disorder[30,31].

The circadian clock is a central regulator of neuronal redox metabolism and excitability in the adult mammalian brain – not only in the suprachiasmatic nucleus (SCN)[32,33] but also hippocampus (HIP)[34]. This is supported by evidence that cortex excitability underlies circadian regulation in humans[35]. Thus, the circadian clock output modulating neuronal excitability is a promising candidate system, that might be involved in mechanisms leading to BD symptoms and recovery.

Cumulative evidence suggests that lithium regulates some of the chronobiological abnormalities in BD as part of its therapeutic action due to its effects on the phase, amplitude, and period of circadian rhythms[36–39]. Of particular interest, both, in vitro and in vivo studies have reported the regulatory effects of lithium on the core clock genes, the molecular machinery that drives circadian rhythms[37,40,41].

Several studies have explored the association of genetic variants in clock genes with lithium response[42–45]. Despite some suggestive results, the implication of clock genes as risk factors for these phenotypes has not yet been firmly established in humans. One potential explanation for these inconclusive results is that genetic association studies primarily aim to estimate the individual effect of each genetic variant rather than analyzing the global contribution of genetic variants in biologically meaningful sets of genes. Gene set analysis holds promise to overcome this limitation by integrating the polygenic architecture of these traits[46] with biological information in association analyses[47].

In this study, we have defined the following gene sets related to circadian rhythm, based on previous empirical evidence: 1) clock modulator genes, 2) core clock genes, and 3) genes with a circadian pattern of expression. We use GWAS summary statistics of major psychiatric disorders, chronotype, and lithium response as the basis for gene set association analyses. We report the significant enrichment of core clock gene sets in lithium response in BD using two different gene set analysis methods (MAGMA and INRICH)[48,49]. We have replicated our findings in an independent GWAS on lithium response. We have identified BHLHE41 as the promising candidate for further investigation. We found that *Bhlhe40/41*$^{-/-}$ double-knockout (DKO) mice are partially non-responsive to lithium's effect on cognitive performance. We have observed altered expression of a postsynapse-regulating gene set in layer 2/3 pyramidal neurons, a reduced excitability in DKO cortical neurons in culture as well as glutamatergic neurons in layer 2/3 of the anterior cingulate cortex (ACC) and the CA1 region of the ventral hippocampus (vHIP) in acute slices. Furthermore, DKO neurons were non-responsive to chronic lithium treatment induced excitability dampening. Finally, we observed reduced LTP in CA1, confirming network level changes of synaptic plasticity in learning and memory-associated brain regions.

Material and Methods

All methods were carried out in accordance with institutional guidelines and regulations including animal experiments approved by the Regierungspräsidium Oberbayern, ROB Munich, Germany under the license ROB-55.2-1-54-2532-179-2016.

Human Genetics

Definition of circadian gene sets

Clock modulator gene set: genes that serve as likely regulators of the core clock based on a genome-wide small interfering RNA (siRNA) screen in a human cellular clock model.[50] The primary hit list included i) double hits (siRNA) for high amplitude, short period and long period, and ii) single hits for high amplitude and short period. Core clock gene sets: genes centrally involved in the cellular time-keeping mechanism[51–53]. Since it is difficult to define a universally accepted consensus list of core clock genes, we opted for three different gene sets ranging from a more restrictive (“core clock minimal”) to a more relaxed (“core clock extended”) definition.

Circadian oscillating/output gene sets: genes that exhibit oscillatory expression but make no known contribution to the core time keeping mechanism. The *Circadian mouse tissues (Yan 2008)* gene set was based on those genes showing a circadian oscillation expression pattern in at least 6 different mouse tissues[54]. The *CircaDB circadian CNS tissues* gene set was based on the data available in CircaDB (http://circadb.hogeneschlab.org/) and included genes showing a circadian expression pattern in at least 4 mouse CNS tissues[55]. The *Circadian human brain (Li 2013)* gene set included the top cyclic genes in the human brain across six different brain areas[56]. Likewise, the *Circadian human prefrontal cortex (Chen 2016)* gene set represented the top 50 clock-regulated genes in the human prefrontal cortex (Brodmann areas 11 and 47)[57]. See Table S1 for a list of the specific genes contained in each gene set.

A curated homology list (Mouse Genome Informatics, The Jackson Laboratory) was used to perform mouse-to-human gene mapping.

Target phenotypes

GWAS summary statistics available for European-origin populations for schizophrenia (SCZ)[58], post-traumatic stress disorder (PTSD)[59], major depressive disorder (MDD)[60], bipolar disorder (BD)[61], autism spectrum disorders (ASD)[62], attention-deficit/hyperactivity disorder (ADHD)[63], chronotype[64], and lithium response defined as continuous or dichotomous trait (ConLiGen)[65]. The sample size of each study is shown in Table S1.

Gene set analyses

The European panel of 1000 Genomes Project, phase 3 was used as reference for all processing/analysis steps. NCBI build 37.3 genomic annotation was used for gene locations.

MAGMA[48] and INRICH[49] were used to carry out competitive gene set analyses. Both methods were chosen because of their good performance in keeping a low type-1 error rate and dealing with confounding factors like gene size, gene density and linkage disequilibrium (LD) between genes[47]. Together they provide complementary approaches because each method captures different facets of the association signal[47]. The built-in procedures for empirical multiple testing correction were not used. Instead, more conservative Bonferroni corrections were used for the set of traits and gene sets after enrichment analyses.

MAGMA analyses (v1.06, https://ctg.cncr.nl/software/magma): After SNP to gene annotation, gene-level analyses were carried out using the 'snpwise-unweighted' model. Gene-based P-values were obtained by combining the SNP P-values in a gene (± 10 kb) into a gene test-statistic (mean $\chi 2$) corrected for LD between SNPs. MAGMA competitive gene set analysis was used for testing, within a regression framework, if the genes in circadian gene sets have a stronger association with the target phenotype than other genes. For gene set competitive testing, linear regression analyses were conditioned to gene size, log(gene size), gene density, log(gene density), inverse mac and log(inverse mac). Gene-gene correlations were also considered in the model.

INRICH analyses (https://atgu.mgh.harvard.edu/inrich/): This permutation-based competitive gene set analysis tool takes a set of genomic regions (intervals) that are independently associated with a trait, and then tests for the enrichment of predefined gene sets. LD-independent associated genomic intervals for each trait were generated using SNP tagging (--tag-kb 1000 --tag-r2 0.2) in PLINK (v1.9)[66]. Intervals were calculated at four different P-value thresholds (P_{TH} = 0.00001, P_{TH} = 0.0001, P_{TH} = 0.001, P_{TH} = 0.01). The next step was to count the number of associated intervals overlapping with genes in the circadian gene sets. Interval overlap was limited to ±10 kb up/downstream of a gene. Random interval sets were generated 10,000 times (first-pass permutations), with each set approximately matching the associated intervals regarding the number of SNPs, overlapping genes, and SNP density per kb. The overlap of circadian gene sets was also determined in these random intervals to generate a distribution of the enrichment statistics for such target gene sets under the null hypothesis. Finally, the empirical P-value was

calculated as the proportion of random replicates where the enrichment statistic is as large as that of the original interval set.

FUMA analyses (http://fuma.ctglab.nl/): The MAGMA implementation in FUMA[67] was used for an unbiased gene set analysis in the ConLiGen dataset. A total of 10,655 predefined gene sets (curated gene sets: 4738, GO terms: 5917) derived from Molecular Signatures Database (MSigDB) v6.1 were included (http://software.broadinstitute.org/gsea/msigdb/index.jsp).

Lithium response: samples and phenotypes

The international Consortium on Lithium Genetics (www.ConLiGen.org) has recruited 2,563 BD patients treated with lithium and includes 22 sites across four continents (Europe, America, Asia and Australia)[65,68,69]. Only European-origin ConLiGen samples (N = 2,343) were used for gene set association (summary statistics) and polygenic analyses (N = 2,153). The "Retrospective Criteria of Long-Term Treatment Response in Research Subjects with Bipolar Disorder" (Alda scale[18]) was used for the evaluation of long-term treatment response to lithium. This scale was designed to assess long-term response, while considering confounding factors. The A score (range 0 – 10) quantifies symptom improvement over the lithium treatment period. The A score is then weighted against five criteria (B score) that assess confounding factors (disease course, compliance, and add-on treatments) each scored 0, 1, or 2. The total score is derived by subtracting the total B score from the A-score. Dichotomous response criteria were defined with a total score ≥ 7 for "responders" (< 7 "non-responders"). The continuous response was defined using A score but excluding subjects with a total B score > 4[68].

Data analysis and visualization

Additional statistical analyses and data management were carried out using R v3.5.0[70] and SPSS v25.[71] Plots were generated using *ggplot2*[72] or *lattice*[73] R packages.

Behavioral Animal Study

Animals and Husbandry

A wildtype colony of C57Bl/6NCrl mice was used for backcrossing. Chow and water were provided *ad libitum*, except for the IntelliCage system-based experiments for spatial learning. *Bhlhe40/41*$^{-/-}$ (DKO) and wildtype (WT) mice were no more than two to three generations apart from litter mates and weaned after three weeks. Both, male and female mice were tested. The experiment mice were kept in type IV cages (Tecniplast 2000, 612 x 435 x 216 mm, 2065 cm²) in groups of litters of 12 to 16 mice. Experiments with young adult mice started at nine weeks (Open Field Test) and ended at 19 weeks (Remote Fear Memory) of age.

Handling and General Experimental Procedures

All experiment mice were handled with handling tunnels, placed in their home cages[74]. All experiments outside of the IntelliCage system (TSE Systems) were conducted during the light phase, randomizing the trials across group to ensure a uniform distribution and excluding circadian effects. For habituation, the home cage was placed in the test room for ten minutes before the actual experiment. Before and after each trial, the arena and other equipment in direct contact with test mice was cleaned with a dilute SDS solution, wiped dry, and disinfected with

70 % ethanol, unless stated otherwise. All behavioral test details have been described previously[75].

Lithium treatment

Starting three weeks before the first behavioral test, mice were treated chronically with 600 mg/L lithium chloride (LiCl) in the drinking water throughout the experiments. Water was available *ad libitum*. No significant differences in drinking behavior were observed between groups when monitored with the IntelliCage system (TSE Systems; see section 0 for details; Figure S2A).

Transponder Implantation

All experiment mice were equipped with an RFID chip for tracking in the IntelliCage and blinded identification throughout the experiments. Before the actual surgery, the neck region was shaved, cleaned with 70 % alcohol for disinfection, and the transponder (1.4 x 11 mm) was injected subcutaneously.

Camera Tracking

The following tests were done using the camera-based tracking software ANY-maze (Stoelting Europe): open field test, Y-maze test, tail suspension test, and fear conditioning test. In addition to the published standard fear conditioning protocol, the mice were placed in the original arena three weeks after the conditioning stage to assess remote context-related fear memory. All other tests were performed essentially as described in detail previously[75,76].

Prepulse Inhibition Test

For the assessment of prepulse inhibition of the startle response to auditory stimuli, we used the SDI Startle Response System and SRLab software (San Diego Instruments).

IntelliCage-Based Tests

For circadian activity tracking, spatial learning tests and the sucrose preference test, we used the IntelliCage system (TSE Systems). The device allows for home cage monitoring in social group and conditioning in four corners, each with a water bottle in a corner. The access to these water bottles can be denied in learning experiments by closing plastic doors, opening it only in case of “correct” nose pokes at the respective door. The tests were run as described[75,76] with the following minor modification: Activity was first assessed in a five-day period, during which the mice were first accustomed to the new environment (two days of free adaptation), the door opening (one day doors opened on visit), and to learn opening the doors by nose poking (two days nose-poke adaptation). After that, mice could access water in only one of the four corners for spatial positive reinforcement learning (two days place learning). Next the corner was changed pseudo-randomly for five days. Finally, one of the two bottles in each corner was filled with 4 % sucrose water for the sucrose preference test (one day).

Data Analysis and Visualization

Data were aggregated and processed using *FlowR* (XBehavior) as the user interface for the PsyCoP bundle[75]. Additionally, R scripts were used to conduct all custom non-pipeline data analyses using *R 4.0.4*[70] in *RStudio IDE* (RStudio). Box and whisker plots and dimension plots

were created with *ggplot2*[77]. Heatmaps were plotted with *pheatmap*[78]*.* A multivariate linear model was fitted and used in a multivariate analysis of variance (ANOVA) from a Wilk's lambda distribution using *car*[79]. Univariate contrasts were derived from the same model. For univariate contrasts with a significant interaction, a unifactorial "simple-effects" ANOVA was computed to independently test the treatment effect for each genotype.

The dimensionality reduction procedure was described in detail earlier[75]. In brief, missing values were imputed using the non-linear iterative partial least squares (NIPALS) algorithm in *ade4*[80]. The resulting reconstituted matrix was used for canonical discriminant analysis (CDA) with *candisc*[81]. CDA provides an optimal solution for group separation in phenotypic space, by finding linear combinations of single variables, called *canonical components,* similar to the *principal components* in a principal component analysis (PCA). Based on the CDA results of the collapsed factors, we generated a dimension plot with overlayed data ellipses, which include 75 % of the respective sample. A heatmap was created, showing the weights (*canonical coefficients*) of each dependent variable in the *canonical component* of each of the three terms (genotype, treatment, and interaction) of the multivariate linear model. Moreover, a CDA was computed for each of the two "simple-effects" models (DKO and WT).

Each variable was classified *a priori* in accordance with the Research Domain Criteria (RDoC) framework[82]. The heatmap was sorted and grouped, accordingly.

Single-Nucleus Transcriptomics

Sample Processing

For single-nucleus RNA sequencing (snRNAseq), mouse brains were isolated at zeitgeber time (ZT) 4, at the minimum of BHLHE41 expression[27], and kept in ice-cold phosphate-buffered solution (PBS; Gibco). Target tissue was isolated from 500 µm slices. Tissue from three mice was collected and pooled. The freshly isolated tissue was homogenized in nucleus isolation buffer (0.32 M sucrose, 3 mM $Mg(Ac)_2$, 5 mM $CaCl_2$, 10 mM Tris-HCl pH 8.1 with 0.1 % Triton-X100 freshly added; all Sigma) with a 2 ml Dounce-type tissue homogenizer. The sample was overlayed on top of a sucrose cushion (1.8 M sucrose, 3 mM $Mg(Ac)_2$, 10 mM Tris-HCl, pH 8.1, all Sigma) and centrifuged at 4 °C and 17,000 x g for 70 min. The supernatant was removed, the pellet washed with PBS and resuspended in resuspension buffer (PBS, 1 % bovine serum albumin (BSA) and 0.04 U/µL Protector RNAse inhibitor; all Sigma). The suspension was passed through 30 µm pre-separation filters (Miltenyi Biotec) and cells were kept in ice-cold resuspension buffer. Small aliquots of the samples were stained with trypan blue and Hoechst 33258 to determine nucleus density, integrity, and multiplet rate in an improved Neumann counting chamber. The nucleus density was adjusted to 2500 nuclei/L (±10 %). Nuclei aggregation rate was significantly below 10 % in all samples.

Library Preparation

Single-cell libraries were prepared with SureCell Whole Transcriptome Analysis 3' Library Prep Kit (Illumina) following the manufacturer's protocol using a ddSEQ Single-Cell Isolator (Bio-Rad). Each sample was run on 4 lanes, assuming a total of approximately 1200 cells per sample.

Average fragment size, quality and yield of the final libraries were assessed on a Bioanalyzer 2100 (Agilent).

Libraries were sequenced at a loading concentration of 3 pM on a NextSeq550 (Illumina) in paired-end mode with 69 cycles Read1, 8 cycles Index1, and 91 cycles Read2.

Upstream Analysis of snRNAseq Data

The BCL files were demultiplexed with *bcl2fastq* (Illumina) and the sequence quality was checked with *FastQC* (v0.11.9). Cell barcodes and unique molecular identifiers (UMIs) were isolated and tagged with *ddSeeker*[83]. After tagging, the data were processed with *Drop-seq* tools (v2.3.0). A metabundle was created using release 102 of the *Ensembl* annotation and the *GRCm38* mouse genome. Corrupted cell barcodes were removed from the data. The reads were sorted by query name, and the data converted back to FASTQ for mapping. Read2 was mapped using *STAR aligner* (v2.7.5)[84] with default settings. Mapped data were merged with barcode-tagged data. The uniquely mapped reads were functionally annotated for counting. Digital gene expression data matrices were created for the 6000 most abundant cell barcodes in each sample. The cut-off was chosen based on the knee plot made with *ddSeeker*'s *make_graphs.R*.

Downstream Analysis of snRNAseq Data

For downstream processing of snRNAseq data, we used the R package *Seurat v4* (v4.0.1)[85]. After import as a matrix, Seurat objects were created for each sample. Only cells with at least 200 features expressed and only features expressed in at least 3 cells were included in the object. Mitochondrial RNA content was determined by grepping for "^MT-" and hemoglobin contamination was quantified by grepping for "^Hb". The cells were filtered for hemoglobin contamination of less than 1 % of the total UMI counts, a minimum of 500 and a maximum of 1100 different expressed features to remove both background or low-quality nuclei and aggregates.

Normalization and Integration of snRNAseq Data

The UMI count data matrices were normalized by the single cell transform procedure (SCTransform)[86]. Both, mitochondrial and hemoglobin transcript contents were regressed out as indicators of RNA background. For integration, we used the reciprocal principal component analysis (rPCA) procedure with the *k.anchor* parameter set to 48.

Dimension Reduction and Clustering of snRNAseq Data

The first 30 principal components (PCs) were computed using the 3000 most variably expressed features. Using all 30 PCs, we performed similar nearest neighbor (SNN) graph-based clustering with a resolution of 0.56. We identified a total of 6 cell clusters. Next, we computed a uniform manifold approximation and projection (UMAP) embedding[87].

Differential Expression Analysis

Differential gene expression was analyzed with *Seurat v4*[85]. Features entering the analysis were filtered for a minimum of 1 % expressing cells in the tested population. The filtered data were normalized but not integrated. The results were tested using the model-based analysis of single-cell transcriptomics (*MAST)* procedure[88] and P-values were Bonferroni corrected. Differentially expressed features going into downstream analysis were filtered for a minimum

average log2-transformed fold-change (avg_log2FC) of 0.1 as low coverage reduces the fold-change due to a high proportion of non-expressing cells.

General Enrichment Analysis and Protein Interaction Network Analysis

For gene annotation enrichment analysis and protein-protein interaction (PPI) network analysis, the Metascape platform[89] was used. Previously identified differentially expressed genes (DEGs) were entered for custom analysis. Default parameters for annotation and membership were used. The background gene set parameter was set to the expressed features in the respective population and only selective gene ontology (GO) clusters were analyzed.

For network analysis, the top 3 candidate genes, CSNK1E, BHLHE41, and RORB, as well as BHLHE41's paralog BHLHE40, were added to the gene list and the network was computed using all databases combined.

Enrichment Analysis of Synapse-Related Gene Ontology Terms

For a more specific enrichment analysis, the SynGO database[90] for synapse related GO annotations was used. The input gene list was extended by relaxing the P-value adjustment and all expressed features in the respective cell population was used as background gene list.

Reporter Assays

Cell culture

Primary cortical neurons were isolated from brains of E15.5 C57BL6/NCrl WT and DKO mice. Cortical tissue was treated with a pre-activated papain suspension (Worthington) and gently dissociated by pipetting. 5×10^5 Cells were plated in neurobasal medium supplemented with 5 % fetal calf serum (FCS), 2 % B27 serum supplement, and 1 % GlutaMax (all Gibco) on 35 mm plastic tissue culture dishes (BD Falcon) coated with poly-D-lysine (MW 70,000 – 150,000; Sigma).

On day *in vitro* (DIV) 1, plating medium was replaced with 1.5 mL culture medium (neurobasal medium, 2 % B27, 1 % GlutaMax). 500 µL culture medium was added on DIV5 and DIV11. The cultures were kept in a humidified incubator at 37 °C and 5 % CO_2.

AAV production

AAV1/2 particles were produced following a previously published protocol[91]. In brief, HEK293FT cells were transfected with the ESARE reporter AAV vector (pAAV-ESARE-Luc2A) and pFdelta6 helper plasmid. A mix of the capsid plasmids pH21 (serotype 1) and pRV1 (serotype 2) was used to produce AAV1/2 mixed serotype particles. Polyethylenimine (PEI) transfection reagent (Polyscience) was used for transfection. Cells were lysed and treated with benzonase (Sigma). The lysate was filtered through a 0.45 µm syringe filter (Millipore) and concentrated using an Amicon Ultra-15 centrifugal filter unit (100 kDa membrane cut-off; Millipore). Each AAV sample was digested with TURBO DNase (Invitrogen) to remove double-stranded copies of the viral genome and successfully packaged AAVs were released by proteinase K (Invitrogen) digestion and isolated by spin column-based purification (Macherey-Nagel). The titer was quantified by qRT-PCR with WPRE primers.

Lentivirus production

In brief, lentiviral particles were produced by co-transfecting HEK293FT cultures with the Bmal1 reporter construct (pLV6-Bmal1p-Luc) together with the VSV-G envelope plasmid pMD2.G and the packaging plasmid psPAX6 using PEI transfection reagent (Polyscience) similar to AAV production. Transfection medium was exchanged for fresh DMEM without FCS and phenol red (Gibco) 4 hours after the transfection mix had been added. Virus-containing supernatant was collected after 24 and 48 hours. Lentiviral particles were purified by centrifugation and filtering through a 0.45 µm syringe filter (Millipore).

Live-cell luciferase assays

Live-cell luciferase recordings were used for ESARE and *Bmal1p* reporter assays. For Bmal1p, primary neuron cultures were infected by seeding in a 1:1 mix of plating medium and purified viral supernatant. On DIV11, cultures were synchronized with forskolin. In brief, half of the supernatant was removed and diluted 1:1 with fresh culture medium. 500 µL of forskolin stock solution (Supelco) was added to a final concentration of 20 µM. After 2 hours, the supernatant was replaced with culture medium supplemented with D-luciferin (P.J.K. Biotech).

For ESARE assays, cultures were infected by adding virus stock to the culture medium on DIV1 (MOI 1000). On DIV5, lithium chloride in PBS or PBS alone was added with 500 µL medium (final concentration 1.5 mM). On DIV11, the supernatant was supplemented with D-luciferin for baseline recordings. After 24 hours, cultures were stimulated by adding 1(*S*),9(*R*)(−)-bicuculline methochloride (BIC) to a final concentration of 50 µM, silenced by adding a mixture of tetrodotoxin (TTX) and (2*R*)-amino-5-phosphonopentanoate (AP-V) at a final concentration of 1 µM (TTX) and 100 µM (AP-V), or mock treated by adding fresh medium (vehicle only). During the recordings all cell cultures were kept in a LumiCycle 32 apparatus inside a dry incubator (37 °C, 5 % CO_2).

Data Analysis

For data analysis in R, the mean signal and the corresponding standard error of each group was computed for plotting with ggplot2[77]. For the boxplots and statistics, the area under the curve (AUC) was approximated using the rolling mean between neighboring datapoints for each sample's stimulation peak and tested by two-way ANOVA using type 2 sum of squares and subsequent simple-effect (one-way) ANOVAs of the treatment effect of each genotype. Since a mean of means was tested and the small sample size of four, no test for normality was conducted.

Electrophysiological recordings

Whole-cell patch-clamp recordings

Slices were prepared as described previously[92]. In brief, mice were decapitated and the isolated brains transferred into ice-cold and pre-oxygenated artificial cerebrospinal fluid (aCSF; buffered solution of 1.25 mM Na_2HPO_4, 125 mM NaCl, 14 mM D-glucose, 2 mM $MgSO_4$, 1.5 mM $CaCl_2$, 2.5 mM KCl, and 26 mM $NaHCO_3$, pH 7.4). 300 µm Slices were cut using a vibratome (VT 1200, Leica). Slices containing either the ACC or the vHIP were transferred into the incubation chambers with oxygenated aCSF (pH 7.4, aerated with 95 % O_2, 5 % CO_2, 32 – 34 °C) for 1 h

recovery period, and then to room temperature aCSF, oxygenated with carbogen at a rate of 4 mL/min.

All whole-cell recordings were performed on pyramidal neurons in the CA1 region in vHIP or pyramidal cells in the cortical layer 2/3 in ACC, as described previously[93,94]. Briefly, pyramidal neurons were identified by morphology. Access resistance was measured before and after recording using transient current responses to 5 mV hyperpolarization pulses. Patches with more than 10 % change in access resistance were excluded from downstream analysis. Additional exclusion criteria were leak currents of less than 150 pA, membrane resistance below 0.8 GΩ, or serial resistance of more than 20 MΩ.

Spontaneous excitatory postsynaptic currents (sEPSCs) were measured at a holding potential of −70 mV. sEPSC recordings in ACC were measured in the presence of 5 µM strychnine and 5 µM BIC. Recording pipettes were filled with recording solution (140 mM potassium gluconate, 0.5 mM Na_2GTP, 4 mM Na_2ATP, 10 mM EGTA, 1 mM $CaCl_2$, and 2 mM $MgCl_2$, buffered with 10 mM HEPES, pH 7.3).

Spontaneous inhibitory postsynaptic currents (sIPSCs) were measured in the presence of 10 µM 6-cyano-7-nitroquinoxaline-2,3-dione (CNQX, Sigma) and 50 µM AP-V. Here, the recording pipettes were filled with recording solution containing 0.5 mM Na_2GTP, 4 mM Na_2ATP, 10 mM EGTA, 140 mM KCl, 1 mM $CaCl_2$, and 2 mM $MgCl_2$, buffered with 10 mM HEPES (pH 7.2).

For mEPSC and mIPSC recordings, 0.5 µM TTX was added to the bath solution.

Long-term potentiation measurements

Long-term potentiation (LTP) recordings were performed as described earlier[95–97]. In brief, transverse hippocampus slices (300 µm) were cut in ice-cold and pre-oxygenated slicing buffer (10 mM glucose, 218 mM sucrose, 3 mM KCl, 0.2 mM $CaCl_2$, 6 mM $MgSO_4$, 1.25 mM NaH_2PO_4, and 26 mM $NaHCO_3$). Slices were transferred to 32 °C warm aCSF oxygenated with carbogen and incubated for 1 h. For field potential recordings, Schaffer collaterals were stimulated in the stratum radiatum at the CA3/CA1 junction. Amplitude (baseline to peak) and slope (20 – 80 % level of the falling phase) of field excitatory post-synaptic potentials (fEPSPs) were quantified. The half-maximum response was defined as baseline fEPSP. Three trains of 1 s 100 Hz high-frequency stimulation (HFS) bouts in 20 s intervals were used for LTP induction. Every 20 s after the last train, the response to extracellular stimulation in the CA1 region was measured for 60 min. We quantified short-term potentiation (STP), defined as the mean response in the first 5 min after HFS, and LTP, defined as mean response in the last 10 min of measurement.

Data Analysis

We quantified mean Amplitude and Frequency of mEPSC, sEPSC, mIPSC, as well as sIPSC in ACC and vHIP whole-cell recordings. Each variable was tested in a two-way ANOVA using type 2 sum of squares and, in case of a significant interaction, subsequent simple-effect (one-way) ANOVAs of the treatment effect for each genotype. Since a mean of means was tested, no test for normality was conducted. The same procedure was used for STP and LTP.

Results

The core clock gene set is strongly associated with lithium response, with a few clock modulator genes, including BHLHE41, driving the effect

MAGMA analyses for nine preselected traits revealed the significant association of the core clock gene set (competitive $P_{corrected} = 0.0046$) with lithium response on a dichotomous scale (ConLiGen GWAS). No other statistically significant gene set enrichments, including bipolar disorder and other psychiatric disease risk, were observed in any of the other traits analyzed (Figure 1A).

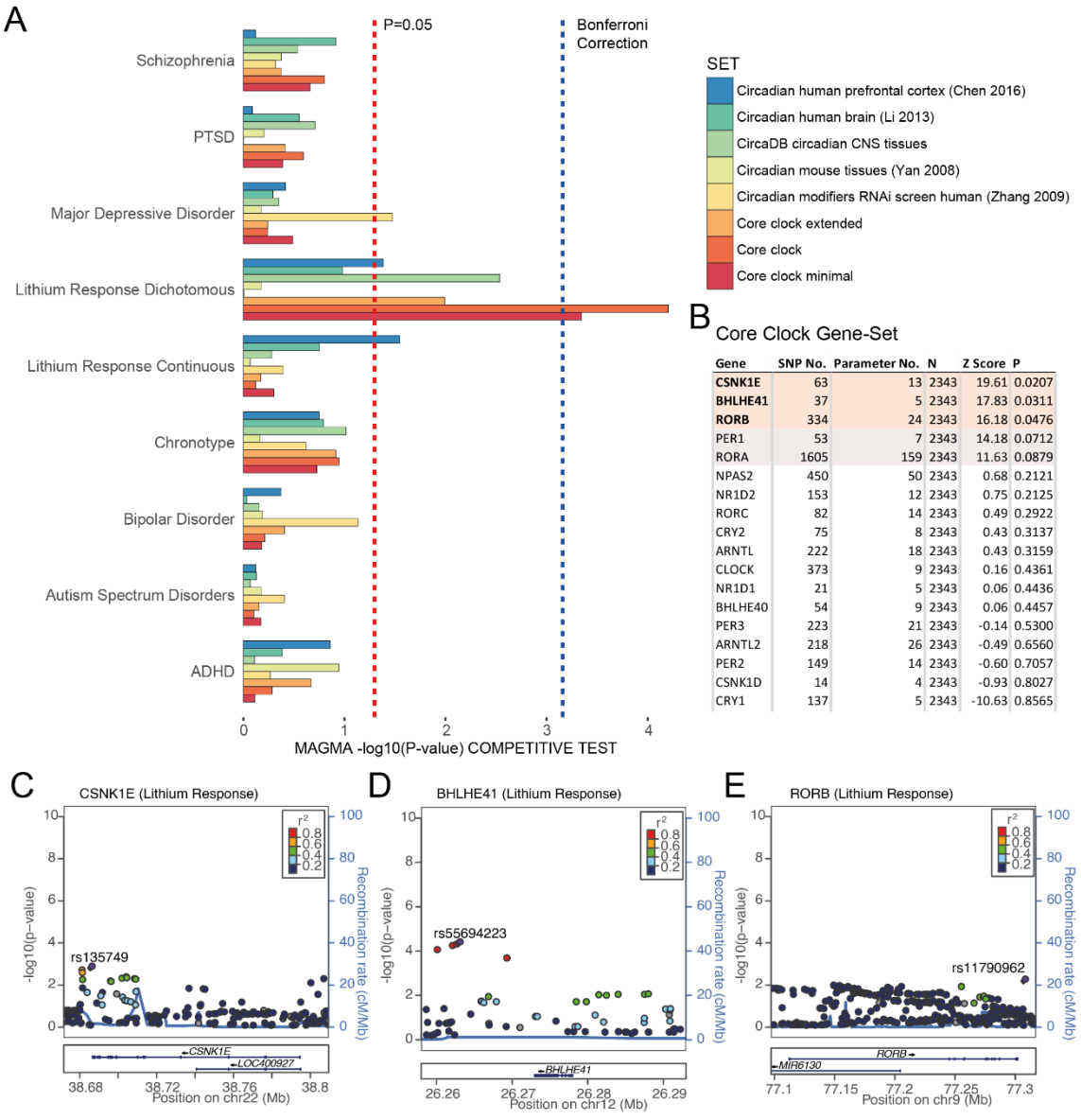

Gene	SNP No.	Parameter No.	N	Z Score	P
CSNK1E	63	13	2343	19.61	0.0207
BHLHE41	37	5	2343	17.83	0.0311
RORB	334	24	2343	16.18	0.0476
PER1	53	7	2343	14.18	0.0712
RORA	1605	159	2343	11.63	0.0879
NPAS2	450	50	2343	0.68	0.2121
NR1D2	153	12	2343	0.75	0.2125
RORC	82	14	2343	0.49	0.2922
CRY2	75	8	2343	0.43	0.3137
ARNTL	222	18	2343	0.43	0.3159
CLOCK	373	9	2343	0.16	0.4361
NR1D1	21	5	2343	0.06	0.4436
BHLHE40	54	9	2343	0.06	0.4457
PER3	223	21	2343	-0.14	0.5300
ARNTL2	218	26	2343	-0.49	0.6560
PER2	149	14	2343	-0.60	0.7057
CSNK1D	14	4	2343	-0.93	0.8027
CRY1	137	5	2343	-10.63	0.8565

Figure 1. BHLHE41 is a strong contributor to the association between lithium response and the core clock gene set. (A) MAGMA analyses based on circadian gene sets in psychiatric traits. Competitive test P-values in the X-axis are –log10 transformed. The dashed blue line indicates the Bonferroni significance threshold ($P < 0.05 / (8 \text{ gene sets} \times 9 \text{ traits})$). The dashed red line indicates the nominal (uncorrected) significance threshold P = 0.05. (B) In gene-based tests, three genes reach nominal significance (depicted in bold, unadjusted P-value). (C – E) Local Manhattan plots of these genes (±15 kb) for dichotomous lithium response show the BHLHE41 locus (D) as the strongest association (5 SNPs with $r^2 > 0.8$) compared to CSNK1E (C) and RORB (E). ADHD: attention-deficit/hyperactivity disorder; PTSD: post-traumatic stress disorder.

Using gene-based tests on the individual member genes of lithium response-associated core clock gene sets, the genes RORB, BHLHE41, and CSNK1E reached nominal significance (uncorrected $P < 0.05$) and the genes PER1 ($P = 0.0712$) and RORA ($P = 0.0879$) were close to significance. These genes, except for PER1, are not components of the core transcriptional-translational loop (TTL) (Figure 1B), suggesting that output genes of the core clock, which regulate metabolic and neuronal activity, might be the major contributors to this association.

The genome-wide gene-based association study (GWGAS) showed that BHLHE41 has the strongest association of the three top genes (Figure 1C – E). In contrast, no such association for BHLHE41 and CSNK1E (all SNPs $r^2 < 0.2$) was found for BD life-time risk, but a strong signal for RORB ($r^2 > 0.8$ and $-\log10(P) > 5$ for lead SNP rs10217741), shown in Figure S1A – C. Of note, BD risk was also not enriched in the MAGMA analyses for any circadian gene set tested (Figure 1D). This strongly suggests that BHLHE41 and CSNK1E are primarily associated with treatment response and neither with pathogenesis of BD nor any other psychiatric disease risk studied.

In addition to MAGMA, INRICH analyses were also computed in order to capture additional types of association. After Bonferroni correction, the dichotomous lithium response was again found to be associated with the core clock gene set ($P_{corrected} = 0.043$ [$P_{TH} = 0.01$]; Figure S1D). The following genes were identified: RORB and BHLHE41 (both also prominent in MAGMA analyses) as well as PER3, ARNTL2 and RORA (Table S1). This enrichment was driven by the overlap of core clock genes with loci associated with dichotomous lithium response at the $P_{TH} = 0.01$ pruning threshold.

Taken together, we found evidence for the association of the core clock gene set, including BHLHE41, as a major driver of lithium treatment outcome but not BD risk using two independent methods of enrichment analysis. This indicates a central role of BHLHE41 in the regulation of disease state in response to treatment but not in neurodevelopmental traits of bipolar disorder or any other psychiatric disease.

Bhlhe40/41$^{-/-}$ double-knockout mice are resistant to lithium's beneficial effect on memory and cognition

After identifying BHLHE41 as a major contributor to the genetic association of circadian clock genes and lithium response in patients, we used *Bhlhe40/41*$^{-/-}$ double-knockout (DKO) mice as a genetic mouse model of altered lithium responsiveness. We focused on DKO mice because they were found to display mixed-state endophenotypes of BD[27] and improved spatial learning and memory consolidation compared to wildtype (WT) mice, whereas *Bhlhe41* and *Bhlhe40* single knockout mice did not[98]. This functional redundancy has also been shown for circadian entrainment and light adaptation phenotypes[99].

Lithium treatment has been shown to increase hippocampal volume in BD patients when compared to non-lithium treated patients[100], to improve cognition and memory performance, and to rescue cognitive dysfunctions in various rodent models[101–105]. Therefore, we conducted a behavioral study using our standardized platform for systematic cognitive and behavioral profiling (PsyCoP) to assess the neuro-cognitive profile of chronically lithium-treated DKO and WT mice

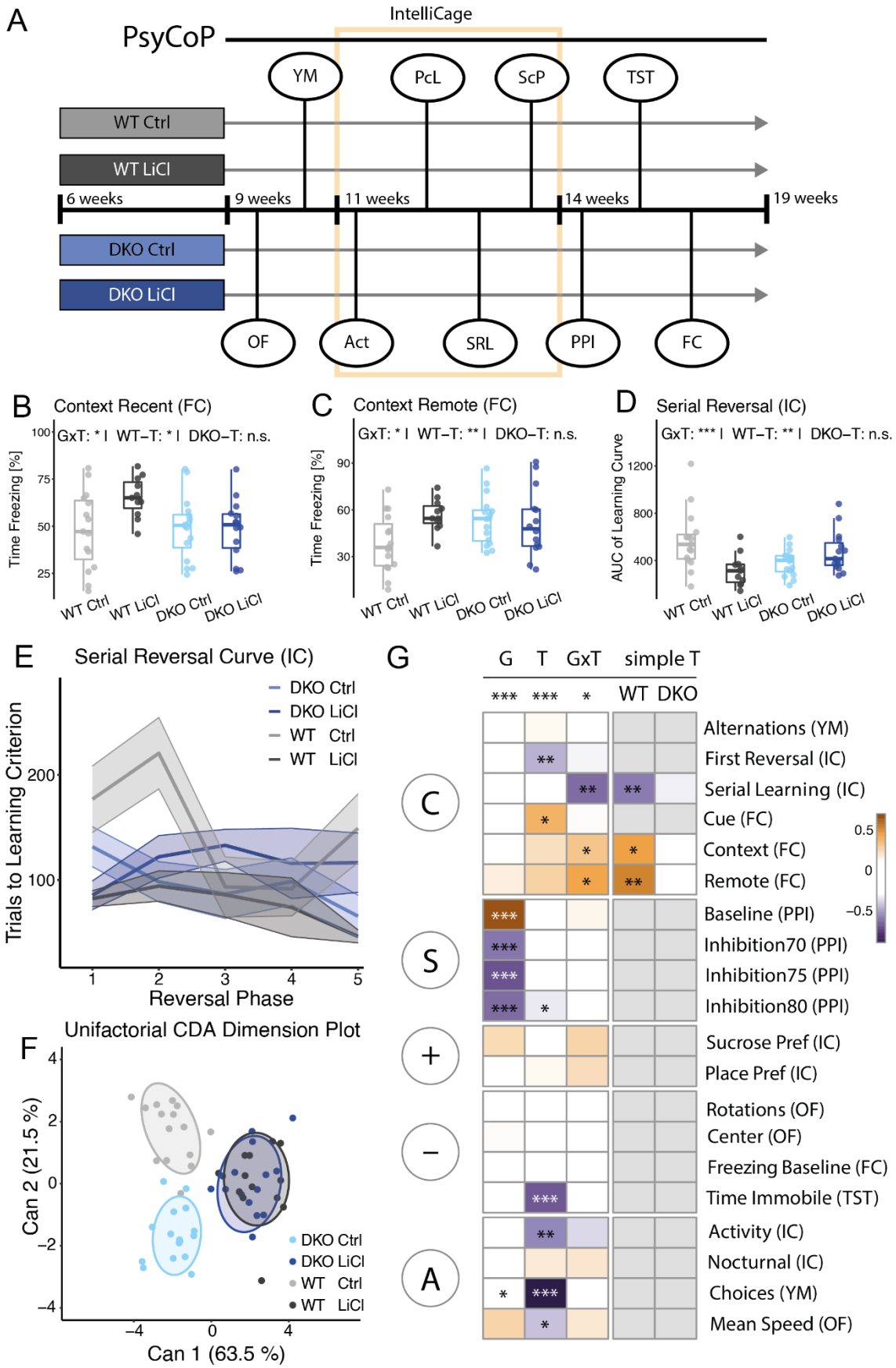

Figure 2. Behavioral profiling reveals non-responsiveness of DKO mice to lithium's beneficial effect on memory and cognition. (A) Schematic of the experimental design. Four groups (genotype × sex) were tested after three weeks of pre-treatment via with either vehicle (Ctrl) or lithium chloride solution (LiCl). Treatment was continued throughout the experiments. (B – D) Boxplots showing that DKO mice are resistant to lithium-mediated effects on spatial reversal learning and contextual fear memory. Data are shown as box

plots with whiskers extending to no more than 1.5-fold IQR. Lithium non-responsiveness was found in (B) recent contextual fear memory, (C) remote contextual fear memory, and (D) serial reversal learning performance as indicated by the area under the learning curve. (E) The ribbon plot of this curve displays the mean number of trials that each group needed to reach the spatial learning criterion after each reversal of the correct corner. Smaller values equal less trials needed and indicate faster learning success. (F) The absence of some lithium effects in DKOs, illustrated by a dimension plot of the canonical scores of the first two canonical components Can1 and Can2 (explaining 63.5 % and 21.5 % of the overall canonical correlation, respectively) from all behavioral data. Data points are highlighted by an ellipse covering 75 % of the sample (upper quartile). (G) The heatmap of the weights of single variables in the structure of the CDA for each term of the profile's linear model. The variables are grouped by RDoC top level domains as assigned *a priori*. Multivariate ANOVA results are shown on top. The main effects might be influenced by the statistical interaction of genotype and treatment. Univariate contrasts reaching significance are indicated with asterisks in the respective panel. * P < 0.05; ** P < 0.01; *** P < 0.001; n.s. not significant; P-values are FDR-adjusted and refer to Wilk's lambda testing two-way ANOVA; simple treatment effects (DKO-T and WT-T) were tested in a similar, but univariate and unifactorial ANOVA procedure; WT: wildtype mice; DKO: BHLHE40/41$^{-/-}$ mice; Ctrl: vehicle control; LiCl: lithium-treated; OF: open field test; YM: Y-maze test; IC: IntelliCage; Act: circadian activity; PcL: place learning; SRL: serial reversal learning; ScP: sucrose preference Test; PPI: prepulse inhibition test; TST: tail suspension test; FC: fear conditioning test; G: genotype main effect; T: treatment main effect; GxT: interaction effect; simple T: simple effects; DKO-T: DKO simple treatment effect; WT-T: WT simple treatment effect; C: cognitive systems domain; S: sensorimotor systems domain; "+": positive valence systems domain; "-": negative valence systems; A: arousal and regulatory systems domain

(Figure 2A)[75]. PsyCoP consists of a series of tests and covers most top-level domains of the Research Domain Criteria (RDoC) system.

Drinking behavior during the IntelliCage period was not significantly different between genotypes as well as treatment groups (Figure S2A).

We detected significant interactions of genotype and treatment (GxT) in the overall PsyCoP profile (MANOVA G: $P = 2.98 \times 10^{-6}$, T: $P = 7.79 \times 10^{-7}$, GxT: $P = 0.0278$; normality controls shown in Figure S2B – C) and in several aspects of the cognitive systems domain (Figure B – E). Contextual fear memory was improved in lithium treated (LiCl) WT mice compared to vehicle control (Ctrl) but not in DKO mice, both short-term (24 hours; Figure 2B; Context: GxT: $P_{adj} = 0.0464$; WT-T: $P = 0.0165$; DKO-T: $P = 0.942$) and long-term (21 days; Figure 2C; Remote: GxT: $P_{adj} = 0.0464$; WT-T: $P = 0.00705$; DKO-T: $P = 0.767$). Similarly, in the serial reversal stage of spatial learning, WT LiCl mice needed less trials to reach the learning criterion, and therefore learned faster than WT Ctrl mice, especially in the first two reversal phases, resulting in significantly smaller area under the learning curve (Figure 2D, E). In contrast, serial reversal learning performance did not improve in DKO mice, resulting in a strong interaction of genotype and treatment, indicating non-responsiveness of DKO mice to the treatment effect (SerialLearn: GxT: $P_{adj} = 0.00248$; WT-T: $P = 0.00675$; DKO-T: $P = 0.0857$).

After CDA dimension reduction (Figure 2F), we observed that ellipsoids of vehicle-treated (Ctrl) DKO mice are clearly different from their wildtype counterpart, whereas lithium treated groups are completely overlapping with a more similar overall response to treatment. When looking at the variable weights (Table S2), it becomes apparent that the shift is mostly driven by the enhancement of cognitive system aspects in WT mice.

A heatmap of variable contributions to the genotype (G), treatment (T), and interaction effects (GxT) shows the RDoC domain-specific character of the non-response to lithium in DKO mice (Figure 2G). In the cognitive systems domain, we find significant interaction for contextual fear memory and serial reversal learning, but not for cue-dependent fear memory (Table S3 and Figure

S3; Cue: GxT: P_{adj} = 0.284). This indicates that the observed non-responsiveness might depend primarily on the ventral hippocampus rather than basolateral amygdala[106].

Sensorimotor gating, on the other hand, was almost exclusively influenced by genotype, with only a minor lithium effect (9.5 % mean decrease) at a prepulse level of 80 dBA (Table S3, Figure S3D – G; Inhibition80: T: P_{adj} = 0.371). Notably, we did not observe lithium treatment effects of aspects of positive and negative valence (Table S3 and Figure S4) except for the time spent immobile in the tail suspension test (TimeImmobile: T: $P_{adj} = 4.44 \times 10^{-6}$). TimeImmobile is likely to be influenced by the general activity level, since arousal and regulatory domains showed a strong reduction in both novelty-induced locomotor activity in the open field (MeanSpeed: G: P_{adj} =0.207, T: P_{adj} = 0.0161, GxT: P_{adj} = 0.298) and Y-maze (Choices: G: P_{adj} = 0.0317, T: $P_{adj} = 5.82 \times 10^{-13}$, GxT: P_{adj} = 0.437) as well as general locomotor activity in the IntelliCage (Activity: G: P_{adj} = 0.0734, T: P_{adj} = 0.00152, GxT: P_{adj} = 0.145), independent of genotype (Figure S5). The only sex-dependent treatment effect was found for general activity, where males showed a stronger reduction in activity level than females (Table S3 and Figure S6; TxS: P_{adj} = 0.0373). Since males and females were kept in separate cages, this might constitute a batch effect for that we cannot control.

In summary, DKO mice were non-responsive to lithium treatment in the cognitive domain, but responsive to lithium treatment for locomotor activity and for negative valence.

Single-cell transcriptomics detects changes in postsynapse-associated genes in layer 2/3 excitatory neurons of the medial prefrontal cortex in DKO mice

DKO mice display alterations in cortex-dependent cognitive processing[98] and the lithium non-response is restricted to the cognitive domain, including learning flexibility, which is associated with the prefrontal cortex in rodents[107] and humans[108]. Therefore, we compared the transcriptional profile of DKO and controls in the medial prefrontal cortex (mPFC) at single-cell resolution (Figure 3A). In order to find relevant constitutive changes that are not modulated by daytime activity, we collected samples on the minimum of *Bhlhe41* expression in mice[109] at zeitgeber time 4.

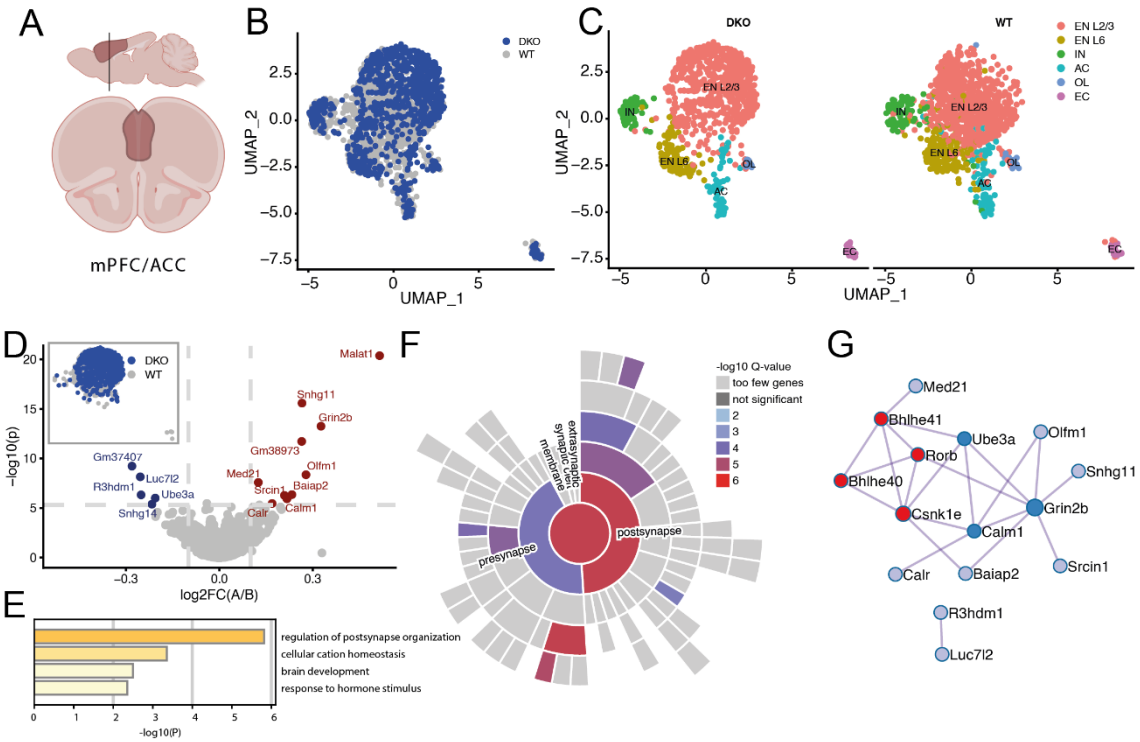

Figure 3. Layer 2/3 excitatory neurons in the mPFC of DKO mice show transcriptional changes in postsynapse-associated genes. (A) The medial prefrontal cortex (mPFC) including anterior cingulate cortex (ACC) was selected as the region of interest and isolated at zeitgeber time (ZT) 4, at the circadian trough of BHLHE41 expression for single-nucleus RNA sequencing (snRNAseq) for identification of constitutively deregulated genes. Created with BioRender.com. (B) UMAP dimension plot of the integrated datasets from wildtype (WT) and *Bhlhe*40/41$^{-/-}$ (DKO) showing successful integration of the samples' transcriptional data. (C) Six major cell populations, shown in distinct colors, were identified in both WT and DKO tissue samples. (D) A Differential expression analysis between WT and DKO Layer 2/3 excitatory neurons (EN L2/3) identified a small set of differentially expressed genes. The gray lines indicate a threshold of 0.1 log2FC (log2-transformed fold-change of average expression between samples) and the Šidak-corrected significance threshold of the −log10-transformed P-value. (E) Gene ontology clusters enriched in the differentially expressed gene (DEG) set find with MetaScape[89] suggest a postsynapse-related mechanism. (F) The enrichment of synapse-related localization ontology clusters in the SynGO database[90] in the nominally significant DEGs supports this finding. (G) The top genes identified in the human GWGAS (red) form a tight protein-protein interaction (PPI) network with the DEGs identified in ACC-derived EN L2/3 (blue) with Grin2b, Calm1, and Ube3a (dark blue) at its center. WT: wildtype mice; DKO: *Bhlhe*40/41$^{-/-}$; EN L2/3: excitatory neurons layer 2/3 (upper layer); EN L6: excitatory neurons layer 6 (deeper layer); IN: inhibitory neurons; AC: astrocytes; OL: oligodendroglial cells; EC: endothelial cells

Clear transcriptional shifts in cell populations between DKO and WT are observed (Figure 3B – C). Based on marker gene expression (Table S4 and Figure S7), we could identify six major cell populations (Figure 3): Layer 2/3 excitatory neurons (EN L2/3), layer 6 excitatory neurons (EN L6), inhibitory neurons (IN), astrocytes (AC), oligodendrocytes (OL), and endothelial cells (EC). When comparing the transcriptional profiles of DKOs and WT in each cell type using differential expression analysis, we found differentially expressed genes only in the EN L2/3 population (Table S4 and Figure 3D). There were no differentially expressed genes found in any other cell type after Šidak correction, except for a significantly lower expression of *Hmgcs2* in endothelial cells (Figure S8). This suggests that the mPFC-associated DKO learning phenotypes primarily depend on pyramidal cells in cortical layer 2/3, which receive monosynaptic input from ventral hippocampus (vHIP) via direct projections to the mPFC, in particular in the prelimbic (PL) and anterior cingulate cortex (ACC)[110,111].

In an enrichment analysis of gene ontology (GO) terms of the differentially expressed gene (DEG) set (Table S4 and Figure 3E), we found “regulation of postsynapse organization” (GO:0099175) to be the top enriched meta feature ($-\log(P) = 5.82$, $q = 0.033$). This was supported by a more focused SynGO localization query, showing enrichment particularly, but not exclusively, for the postsynapse (Figure 3F). Notably, the three genes BHLHE41, RORB, and CSNK1E, which were associated with lithium response, are directly connected with the set of DEGs in a dense interaction network (Table S4 and Figure 3G), supporting a functional link between an altered postsynapse regulation in mPFC pyramidal cells and lithium response.

In conclusion, we found evidence for a change in transcription of genes involved in postsynapse organization of *Bhlhe41/40* expression in layer 2/3 neurons in the mPFC of DKO compared to WT mice.

Primary cortical neuron cultures and principal neurons in ACC and vHIP of DKO mice are less responsive to lithium’s dampening effect on neuronal excitability and plasticity

Lithium has been shown to reduce excitability in lithium-responsive patient-derived neurons, but not in neurons derived from lithium non-responsive patients[17]. Moreover, *Bhlhe41* and *Bhlhe40* expression are induced by neuronal activity[112]. Together with the transcriptional changes that we have observed in DKO L2/3 pyramidal cells, this suggests that lithium response may depend on the regulation of excitability and plasticity in glutamatergic neurons.

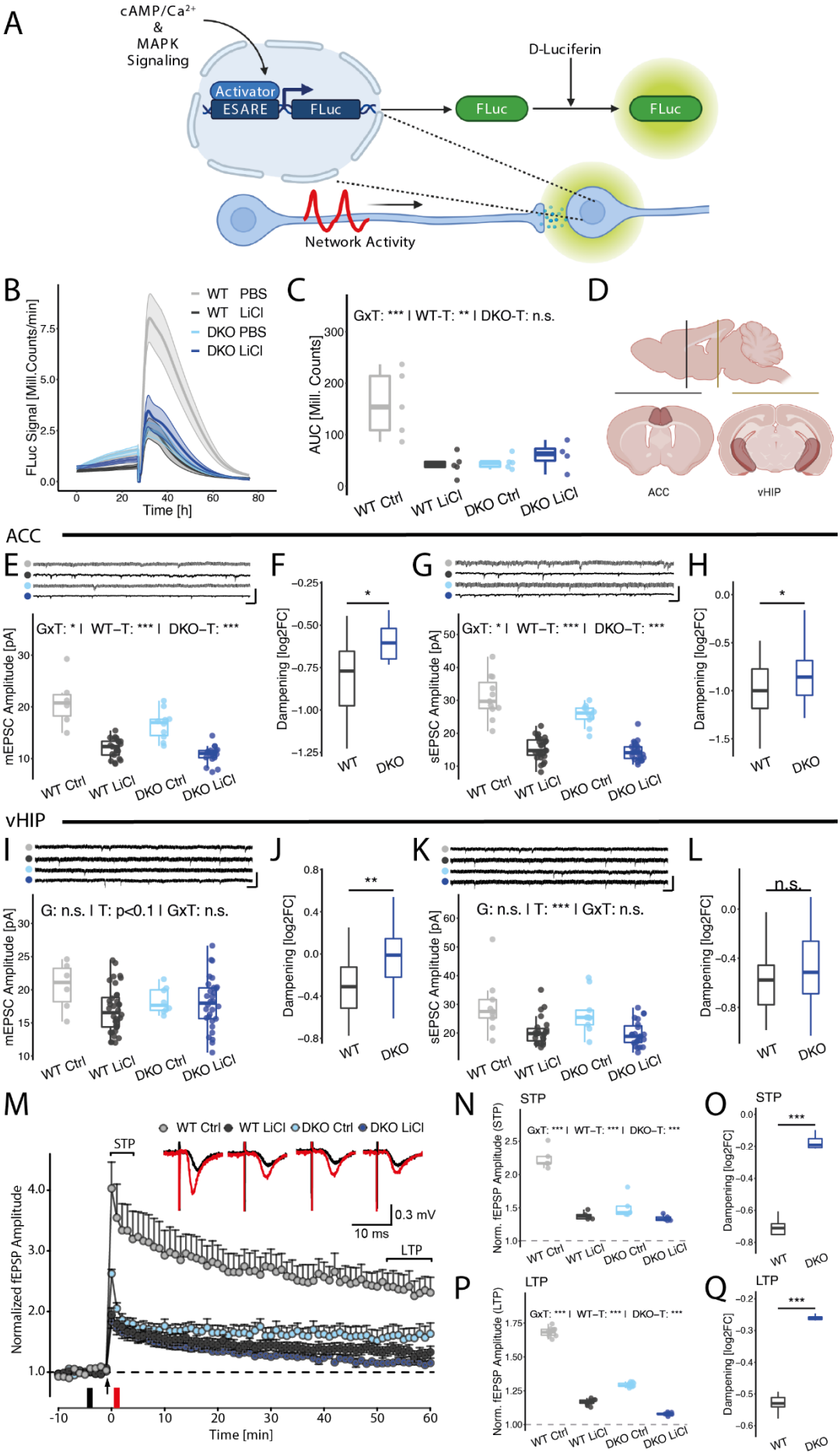

Figure 4. Cortical and hippocampal neurons from DKOs are less responsive to lithium's dampening effect. (A) Neuronal network activity in primary cortical neuron cultures was measured

using a previously published[91] luciferase reporter assay. This transcriptional assay for *cis*-regulatory element activity is based on the "enhanced synaptic activity response element (ESARE) sensor for synapse-to-nucleus signaling. Created with BioRender.com. (B) Ribbon plots of the mean ESARE activity in response to bicuculline (BIC) stimulation after 24 hours. The ribbons indicate the standard error of the mean. (C) Quantification of the stimulation peak; Box plots with whiskers extending to no more than 1.5-fold interquartile range (IQR). Asterisks denote statistical significance of the interaction effect and simple effects for both genotypes tested in a two-way ANOVA. (D) Brain regions for electrophysiology in acute slices were the anterior cingulate cortex (ACC) portion of the medial prefrontal cortex (mPFC) and the ventral Hippocampus (vHIP). Created with BioRender.com. Excitatory postsynaptic current (EPSC) amplitudes were quantified in mPFC (E – H) and vHIP (I – L) and are shown as boxplots with example traces. The scale bars denote 0.2 s in on the X-axis and 0.1 nA on the Y-axis. Average (E) Miniature EPSC (mEPSC) amplitudes and (G) spontaneous EPSC (sEPSC) amplitudes in L2/3 mPFC excitatory neurons. (F, H) Boxplots of the log2-transformed foldchange (log2FC) reduction in LiCl-treated compared to Ctrl-treated neurons in both mEPSC (F) and sEPSC (H) amplitude. (I) Average mEPSC amplitude in CA1 principal neurons. (J) However, the nominal reduction in amplitude is stronger in WT compared to DKO. (K) The average sEPSC amplitude is reduced in both WT and DKO CA1 neurons in response to lithium treatment. (L) But after normalization to the mean amplitude in Ctrl treated mice, there is no significant difference. (M) Short-term (STP) and long-term potentiation (LTP) was assessed by high frequency stimulation (HFS) of the Schaffer collaterals and measuring fEPSP in the CA1 region of the hippocampus. The time point of stimulation is marked by an arrow. fEPSP amplitude was normalized to baseline. (N) The magnitude of STP, determined as maximal responses within the first 5 min after HFS, is significantly lower in DKO mice. (O) When normalized to mean STP in Ctrl treated mice, log2FC reduction of STP amplitude is larger in wildtypes compared to DKO mice. (P) Magnitude of LTP, determined as responses between 50 and 60 min after HFS, is lower in DKO mice. (Q) When normalized to the mean LTP in Ctrl treated mice, log2FC reduction of LTP amplitude is significantly larger in wildtypes compared to DKO mice. * $P < 0.05$; ** $P < 0.01$; *** $P < 0.001$; n.s. not significant; P-values refer to univariate two-way ANOVA with type 2 sum-of-squares; simple effects were tested in a similar but unifactorial ANOVA procedure; WT: wildtype mice; DKO: *Bhlhe*40/41$^{-/-}$ mice; Ctrl: vehicle control; LiCl: lithium-treated; G: genotype main effect; T: treatment main effect; GxT: interaction effect; simple T: simple effects; DKO-T: DKO simple treatment effect; WT-T: WT simple treatment effect.

To test excitability in primary neuronal cultures, we used a previously published transcriptional reporter system for neuronal network activity[91] (Figure 4A). It consists of a firefly luciferase reporter cassette that is coupled to a sensor consisting of clustered *cis*-regulatory elements, the "enhanced synaptic activity response element" (ESARE), that measures synapse-to-nucleus signaling.

This sensor construct was transduced via AAV infection and cultures were pre-treated with lithium and vehicle for one week prior to the measurement. After baseline recording, we stimulated the culture with bicuculline, a competitive $GABA_A$ receptor inhibitor[96] and quantified the peak (Figure 4B-C). We found a highly reduced excitability of DKO neuron cultures and a dampening of the bicuculline response after lithium treatment only in WT neurons, whereas DKO neurons were non-responsive (GxT: $P = 0.00196$; WT-T: $P = 0.00479$; DKO-T: $P = 0.375$). To confirm that this reduced signal was caused by reduced neuronal network activity and not cytotoxic effects of lithium chloride, we silenced lithium-treated WT neuron cultures with a cocktail of TTX and AP-V, which fully eliminated the dampening effect (Figure S9A). Moreover, the molecular clock is still functional in DKO neurons as demonstrated by transducing a Bmal1p controlled luciferase reporter construct and synchronizing the neurons with forskolin (Figure S9B). This supports the hypothesis of a constitutive change in excitability rather than circadian regulation.

To elucidate lithium responsiveness in a more physiological context, we did whole-cell recordings on acute brain slices in two regions of interest that are associated with cognition: the ACC region of the mPFC and the CA1 region in the vHIP (Figure 4D). The mice were chronically treated for at least three weeks with LiCl or vehicle (Ctrl) via drinking water before the first recordings.

Based on our findings in single-cell transcriptomics, we first focused on layer 2/3 pyramidal cells in the ACC. In these cells, we found that mEPSC and sEPSC amplitudes were dampened in lithium-treated WT and DKO pyramidal cells (Figure 4E, G). However, for miniature and spontaneous EPSCs there was a statistically significant interaction of genotype and treatment (mEPSC: GxT: $P = 0.0364$; sEPSC: GxT: $P = 0.0309$), demonstrating a reduced lithium effect in DKO neurons. This was confirmed by normalizing to the respective vehicle control, showing a reduced dampening in DKO ACC slices compared to WT (Figure 4F, H; mEPSC: $P = 0.0178$).

In CA1 pyramidal cells, spontaneous but not mEPSC amplitudes were reduced in slices from lithium-treated mice (Figure 4I, K; mEPSC: T: $P = 0.0822$, GxT: $P = 0.129$; sEPSC: T: $P = 9.82 \times 10^{-6}$, GxT: $P = 0.630$) with no significant interaction effects. However, after normalization to the mean of vehicle-treated slices, we did find a significantly weaker dampening of the mEPSC amplitude in DKO neurons compared WT (Figure 4J; $P = 0.00195$), but no significant difference in sEPSC reduction (Figure 4L; $P = 0.495$). This also reflects a partial lithium non-responsiveness for the dampening effect on excitability, similar to that observed in cortical cultures.

No such effects were found for mIPSC and sIPSC amplitude both in ACC and vHIP recordings (Figure S10A - H), indicating that the difference in bicuculline response found in cortical cultures was not due to changes in GABAergic activity. Not only the amplitude, but also the frequency of DKO Ctrl pyramidal neuron mEPSCs and sEPSCs as well as mIPSC and sIPSC both in ACC and vHIP were reduced compared to WT Ctrl (Figure S10I – L).

To investigate changes in synaptic plasticity, we recorded long-term potentiation (LTP) in the CA1 region of the vHIP, which sends projections to the mPFC[106] (Figure 4N – R). Here, we could see a reduced potentiation of fEPSP amplitude in DKO slices compared to WT as well as a dampening of similar magnitude in slices of WT lithium treated mice (Figure 4N). The input-output function did not reveal changes in synaptic transmission (Figure S11). We also found a significant interaction of genotype and treatment for both short-term (STP) and long-term potentiation (Figure 4O and Q; STP: GxT: $P = 1.36 \times 10^{-22}$, LTP: GxT: $P = 1.27 \times 10^{-5}$). This is reflected by a significantly reduced dampening in response to LiCl in DKO slices compared to WT (Figure 4P and R; STP: $P = 3.27 \times 10^{-7}$; LTP: $P = 8.82 \times 10^{-17}$).

In summary, we could show that lithium treatment lowered the excitability of WT cortical neurons, whereas DKO neurons were partially non-responsive. Moreover, we found that DKO pyramidal cells are less responsive but not immune to lithium induced reduction in mEPSC and sEPSC amplitude. The same effect was seen in LTP in the CA1 region of the hippocampus, reflecting the non-responsiveness of DKO mice to lithium's effect on mPFC-vHIP-dependent learning and memory.

Discussion

In this study, we have applied gene set enrichment methods to identify groups of genes relevant to lithium therapy outcome. Our results suggest a significant role of core clock genes in

the clinical response to lithium in BD patients. These results agree with clinical, physiological, and molecular evidence of the chronobiological effects of lithium and provide novel insights in the pharmacogenomic determinants of lithium response in BD. Although our results confirm a global influence of core clock genes on lithium response, some specific genes seem to have an especially profound influence on these effects: The gene RORB (9q21.13; RAR Related Orphan Receptor B) is a member of the NR1 subfamily of nuclear hormone receptors[51]. It binds as a monomer to ROR response elements and plays a key role in the regulation of the period length and stability of the circadian rhythm. BHLHE41 (12p12.1; also known as SHARP1 or DEC2) codes for a transcriptional repressor that regulates the activity of clock and clock-controlled genes. Mutations in this gene reduce sleep length in humans[113] and Bhlhe40/41$^{-/-}$ double-knockout (DKO) mice are characterized by an altered sleep pattern, with memory and physiological/behavioral features resembling those observed in psychiatric disorders[27,98].

The identification of the core clock enrichment using two different analysis methods, MAGMA and INRICH, that are each sensitive to different types of associations[48,49], supports the robustness of our findings. The results obtained with both analyses indicate that the enrichment of the core clock set involves not only some highly associated genes but also a general trend for association of the whole gene set. One of the main drivers of association found with both methods was the gene BHLHE41.

Therefore, we chose BHLHE41 as candidate for a translational study. We treated DKO mice and wildtype (WT) controls either with lithium chloride (LiCl) or vehicle (Ctrl) via drinking water and characterized the animals in our standardized cognitive and behavioral test battery PsyCoP, followed by an RDoC-based analysis.

We found non-responsiveness to lithium in DKO mice in behavioral domains that are dependent on vHIP-mPFC/ACC interactions, particularly in contextual fear memory[106,114,115] and spatial reversal learning[107,116]. Notably, we did not see such an effect in recent cued fear memory, which was shown to be dependent on basolateral amygdala (BLA) but not vHIP function[117].

ACC and hippocampus are known to be involved in BD pathology, e.g. BD patients have reduced ACC grey matter volume[118,119] and reduced hippocampal volume[120]. Interestingly, hippocampus and cortical grey matter thickness were increased in lithium-treated patients compared to other BD patients[100,121], whereas no increase in grey matter thickness was found in antipsychotic and anticonvulsant-treated patients. Although the functional implications of these findings are not yet clear, they were considered to be proof of the neuroprotective effect of lithium treatment in patients[100,121].

As mentioned above, the neuroprotective effect relates mostly to *in vitro* data, e.g. the non-responsiveness of long-term lithium-treated excitatory neuron cultures to excitotoxicity[13,122]. These findings are in line with the reduced ESARE signal that we found in response to stimulation in primary cortical neurons. It indicates an already lowered level of excitability in DKO cortical neurons that was not reduced further by lithium treatment. The ESARE transcriptional sensor consists of a clustered conserved enhancer of the *Arc* gene[91]. The synaptic activity response element can be found in contains binding sites for SRF/TCF, MEF2, as well as CREB, and is

thought to integrate the most important neuronal activity and plasticity regulating pathways[91,123,124]. We could validate the dampened neuronal excitability in acute brain slices, finding smaller mEPSC and sEPSC amplitudes in layer 2/3 ACC and CA1 pyramidal cells in DKO slices as well as a reduced dampening effect of chronic lithium treatment.

Interestingly, mEPSC and sEPSC frequencies were also lower in control DKO slices compared to WT but came back to WT levels in lithium treated samples. These findings suggest that the response of DKO pyramidal cells to lithium was not only reduced, but fundamentally different from WT pyramidal cells, likely resulting in a difference in synaptic plasticity and producing network level changes different from WT.

In support of these observations, BHLHE41 and BHLHE40 were associated with daytime neuronal activity regulation in the past[99,109]. The transcription of BHLHE40 was also found to be induced in response to Kainate in rat cerebral cortex[112] and a knockdown dampened synapse-to-nucleus signaling in a previously published ESARE assay[91]. Furthermore, DKO mice were found to exhibit a dampened circadian immediate early gene (IEG) expression amplitude in the cortex[27]. Of note, acute lithium treatment was found to increase CRE/CREB-driven transcriptional activity *in vitro* [125] and *in vivo*[126,127], whereas only chronic treatment was shown to reduce CREB activity in mPFC and HIP of a CRE-reporter mouse line[126], reflecting the oppositional effects of lithium short and long-term treatment on neuronal excitability. CREB activation by phosphorylation is regulated by a vast network integrating cAMP/calcium and MAPK signaling[128]. Three previously identified direct targets of lithium, inositol monophosphatases (IMP) as well as polyphosphatases (IPP), adenylate cyclase, and GSK3β*,* are part of this network[129,130]. Based on our findings, CREB could be the point of convergence for lithium's molecular actions, and the key for its therapeutic activity. There is also evidence for the regulation of the core clock by lithium's effect on inositol phosphate signaling and GSK3β regulation[131]. Moreover, lithium-mediated inhibition of GSK3β was linked to changes in dendritic spine organization via cytoskeletal components[132], suggesting several points of interaction revolving around excitability and neuronal plasticity. However, the relationship of lithium's molecular actions remain to be elucidated. Notably, CREB is a central regulator of synaptic plasticity and learning[133]. In fact, chronic lithium treatment was not only shown to rescue increased CRE-driven transcriptional activity in a psychosocial stress model[126], but also the fear memory deficit induced by social defeat[101].

This is now supported by our observation of reduced LTP amplitude in the CA1 region of vHIP in response to lithium treatment. Also, the lithium response amplitude was dramatically smaller in DKO CA1, linking the non-responsiveness to lithium treatment of DKO neurons in culture directly to learning performance. The relevance for BD treatment is further supported by non-responsiveness of induced hippocampal neuron cultures from BD patients to sub-chronic lithium treatment[17].

We found differential expression of postsynapse-regulating genes in layer 2/3 pyramidal cells between DKO and WT mice in the mPFC. This goes in line with the reduction in ESARE activity in cortical neuron cultures. Considering the improved memory consolidation and reduced level of MAPK activity in DKO ACC found in a previous study[98], these observations suggest that the loss

of *Bhlhe40* and *Bhlhe41* function leads to a dampening of neuronal excitability, resulting in constitutive changes in neuronal plasticity in vHIP and mPFC.

In summary, these observations suggest that some of the many actions of lithium come together to modulate excitability, which is already reduced in DKO mice, giving rise to the observed non-responsiveness. Moreover, BHLHE41 is part of the interface between the core molecular clock and a cortical activity-regulating signaling network, including the IEG response[27]. This suggests that the neuronal excitability modulating output of the circadian core clock is of major relevance to the therapeutic effect of lithium salts via tuning synaptic plasticity in the cortex and vHIP.

The details of the underlying molecular mechanisms and the roles of the other top-hit genes in the core clock gene set remain to be investigated in future studies. In addition, all behavioral, molecular, and electrophysiological results were obtained in a genetic mouse model. To fill in the translational gap, we will conduct a validation study in BD patient-derived cortical excitatory neuron cultures. In addition, we will manipulate the gene dosage of BHLHE41 and the other top-hit genes with aim of modulating lithium responsiveness of the cultured neurons. In addition, these patient-derived cultures might offer another powerful tool for future pharmacological research and development, helping to overcome lithium non-responsiveness in BD patients.

Author Contributions

MS performed behavioral tests, single-cell transcriptomics, reporter assays and data analyses. SP conducted the human genetical analyses. MZ conducted the electrophysiological experiments. NJ contributed conceptually and helped with the behavioral setup. ES and PF contributed to the human genetics study and gave conceptual input. TS devised the human genetics study. MJR devised the translational study and contributed to data analysis. WZ supervised the electrophysiological experiments. All authors contributed to the writing of the manuscript.

Funding

MJR is supported by grants from the German Research Foundation (FKZ RO 4076/5-1 and RO 241/16-1). MS is a fellow of the International Max Planck Research School for Translational Psychiatry (IMPRS-TP).

Acknowledgments

We like to acknowledge the contribution of all members of International Consortium of Lithium Genetics (ConLiGen; http://www.conligen.org/) for open access and release of their data, which was essential for this study. We thank Jessica Bly and Wilma Vogel for their support in behavioral experiments and animal keeping. We thank Florian Raabe for conceptual discussions on the translational value of the RDoC framework.

Data Availability Statement

All protocols, scripts, raw and processed data generated for this study will be published on GitHub upon submission to a journal. Scripts will be available as standalone R scripts and as a FlowR bundle.

References

1. GBD 2019 Diseases and Injuries Collaborators. Global burden of 369 diseases and injuries in 204 countries and territories, 1990-2019: a systematic analysis for the Global Burden of Disease Study 2019. *Lancet Lond. Engl.* **396**, 1204–1222 (2020).
2. Plans, L. *et al.* Association between completed suicide and bipolar disorder: A systematic review of the literature. *J. Affect. Disord.* **242**, 111–122 (2019).
3. Del Matto, L. *et al.* Lithium and suicide prevention in mood disorders and in the general population: A systematic review. *Neurosci. Biobehav. Rev.* **116**, 142–153 (2020).
4. Alda, M. Lithium in the treatment of bipolar disorder: pharmacology and pharmacogenetics. *Mol. Psychiatry* **20**, 661–670 (2015).
5. Papiol, S., Schulze, T. G. & Alda, M. Genetics of Lithium Response in Bipolar Disorder. *Pharmacopsychiatry* **51**, 206–211 (2018).
6. Malhi, G. S., Gessler, D. & Outhred, T. The use of lithium for the treatment of bipolar disorder: Recommendations from clinical practice guidelines. *J. Affect. Disord.* **217**, 266–280 (2017).
7. Post, R. M. Acquired lithium resistance revisited: Discontinuation-induced refractoriness versus tolerance. *J. Affect. Disord.* **140**, 6–13 (2012).
8. Akkouh, I. A. *et al.* Exploring lithium's transcriptional mechanisms of action in bipolar disorder: a multi-step study. *Neuropsychopharmacol. Off. Publ. Am. Coll. Neuropsychopharmacol.* **45**, 947–955 (2020).
9. Alda, M., Grof, P., Rouleau, G. A., Turecki, G. & Young, L. T. Investigating responders to lithium prophylaxis as a strategy for mapping susceptibility genes for bipolar disorder. *Prog. Neuropsychopharmacol. Biol. Psychiatry* **29**, 1038–1045 (2005).
10. Vecera, C. M., Fries, G. R., Shahani, L. R., Soares, J. C. & Machado-Vieira, R. Pharmacogenomics of Lithium Response in Bipolar Disorder. *Pharm. Basel Switz.* **14**, 287 (2021).
11. Madison, J. M. *et al.* Characterization of bipolar disorder patient-specific induced pluripotent stem cells from a family reveals neurodevelopmental and mRNA expression abnormalities. *Mol. Psychiatry* **20**, 703–717 (2015).
12. Butler-Munro, C., Coddington, E. J., Shirley, C. H. & Heyward, P. M. Lithium modulates cortical excitability in vitro. *Brain Res.* **1352**, 50–60 (2010).
13. Nonaka, S., Hough, C. J. & Chuang, D. M. Chronic lithium treatment robustly protects neurons in the central nervous system against excitotoxicity by inhibiting N-methyl-D-aspartate receptor-mediated calcium influx. *Proc. Natl. Acad. Sci. U. S. A.* **95**, 2642–2647 (1998).
14. Dixon, J. F. & Hokin, L. E. Lithium acutely inhibits and chronically up-regulates and stabilizes glutamate uptake by presynaptic nerve endings in mouse cerebral cortex. *Proc. Natl. Acad. Sci. U. S. A.* **95**, 8363–8368 (1998).
15. Manji, H. K. & Lenox, R. H. Signaling: cellular insights into the pathophysiology of bipolar disorder. *Biol. Psychiatry* **48**, 518–530 (2000).
16. Ahrens, B., Müller-Oerlinghausen, B. & Grof, P. Length of lithium treatment needed to eliminate the high mortality of affective disorders. *Br. J. Psychiatry. Suppl.* 27–29 (1993).

17. Mertens, J. *et al.* Differential responses to lithium in hyperexcitable neurons from patients with bipolar disorder. *Nature* **527**, 95–99 (2015).

18. Grof, P. *et al.* Is response to prophylactic lithium a familial trait? *J. Clin. Psychiatry* **63**, 942–947 (2002).

19. Geoffroy, P. A. *et al.* Sleep in patients with remitted bipolar disorders: a meta-analysis of actigraphy studies. *Acta Psychiatr. Scand.* **131**, 89–99 (2015).

20. Ng, T. H. *et al.* Sleep-wake disturbance in interepisode bipolar disorder and high-risk individuals: a systematic review and meta-analysis. *Sleep Med. Rev.* **20**, 46–58 (2015).

21. De Crescenzo, F., Economou, A., Sharpley, A. L., Gormez, A. & Quested, D. J. Actigraphic features of bipolar disorder: A systematic review and meta-analysis. *Sleep Med. Rev.* **33**, 58–69 (2017).

22. Milhiet, V. *et al.* Circadian abnormalities as markers of susceptibility in bipolar disorders. *Front. Biosci. Sch. Ed.* **6**, 120–137 (2014).

23. Abreu, T. & Bragança, M. The bipolarity of light and dark: A review on Bipolar Disorder and circadian cycles. *J. Affect. Disord.* **185**, 219–229 (2015).

24. Sylvia, L. G. *et al.* Sleep disturbance in euthymic bipolar patients. *J. Psychopharmacol. Oxf. Engl.* **26**, 1108–1112 (2012).

25. Godin, O. *et al.* Sleep quality, chronotype and metabolic syndrome components in bipolar disorders during the remission period: Results from the FACE-BD cohort. *Chronobiol. Int.* **34**, 1114–1124 (2017).

26. Benard, V. *et al.* Sleep and circadian rhythms as possible trait markers of suicide attempt in bipolar disorders: An actigraphy study. *J. Affect. Disord.* **244**, 1–8 (2019).

27. Baier, P. C. *et al.* Mice Lacking the Circadian Modulators SHARP1 and SHARP2 Display Altered Sleep and Mixed State Endophenotypes of Psychiatric Disorders. *PLoS ONE* **9**, (2014).

28. Schnell, A. *et al.* Mice lacking circadian clock components display different mood-related behaviors and do not respond uniformly to chronic lithium treatment. *Chronobiol. Int.* **32**, 1075–1089 (2015).

29. Mukherjee, S. *et al.* Knockdown of Clock in the ventral tegmental area through RNA interference results in a mixed state of mania and depression-like behavior. *Biol. Psychiatry* **68**, 503–511 (2010).

30. Bellivier, F., Geoffroy, P.-A., Etain, B. & Scott, J. Sleep- and circadian rhythm-associated pathways as therapeutic targets in bipolar disorder. *Expert Opin. Ther. Targets* **19**, 747–763 (2015).

31. Lyall, L. M. *et al.* Association of disrupted circadian rhythmicity with mood disorders, subjective wellbeing, and cognitive function: a cross-sectional study of 91 105 participants from the UK Biobank. *Lancet Psychiatry* **5**, 507–514 (2018).

32. Wang, T. A. *et al.* Circadian Rhythm of Redox State Regulates Excitability in Suprachiasmatic Nucleus Neurons. *Science* **337**, 839–842 (2012).

33. Bothwell, M. Y. & Gillette, M. U. Circadian redox rhythms in the regulation of neuronal excitability. *Free Radic. Biol. Med.* **119**, 45–55 (2018).

34. Kouzehgarani, G. N., Bothwell, M. Y. & Gillette, M. U. Circadian rhythm of redox state regulates membrane excitability in hippocampal CA1 neurons. *Eur. J. Neurosci.* **0**,.

35. Ly, J. Q. M. *et al.* Circadian regulation of human cortical excitability. *Nat. Commun.* **7**, 11828 (2016).

36. McCarthy, M. J. *et al.* Chronotype and cellular circadian rhythms predict the clinical response to lithium maintenance treatment in patients with bipolar disorder. *Neuropsychopharmacology* **44**, 620–628 (2019).

37. Moreira, J. & Geoffroy, P. A. Lithium and bipolar disorder: Impacts from molecular to behavioural circadian rhythms. *Chronobiol. Int.* **33**, 351–373 (2016).

38. Klemfuss, H. Rhythms and the pharmacology of lithium. *Pharmacol. Ther.* **56**, 53–78 (1992).

39. Geoffroy, P. A., Samalin, L., Llorca, P.-M., Curis, E. & Bellivier, F. Influence of lithium on sleep and chronotypes in remitted patients with bipolar disorder. *J. Affect. Disord.* **204**, 32–39 (2016).

40. Yin, L., Wang, J., Klein, P. S. & Lazar, M. A. Nuclear receptor Rev-erbalpha is a critical lithium-sensitive component of the circadian clock. *Science* **311**, 1002–1005 (2006).

41. McCarthy, M. J. *et al.* Genetic and clinical factors predict lithium's effects on PER2 gene expression rhythms in cells from bipolar disorder patients. *Transl. Psychiatry* **3**, e318 (2013).

42. Oliveira, T. *et al.* Genetic polymorphisms associated with circadian rhythm dysregulation provide new perspectives on bipolar disorder. *Bipolar Disord.* **20**, 515–522 (2018).

43. Budde, M., Degner, D., Brockmöller, J. & Schulze, T. G. Pharmacogenomic aspects of bipolar disorder: An update. *Eur. Neuropsychopharmacol. J. Eur. Coll. Neuropsychopharmacol.* **27**, 599–609 (2017).

44. Rybakowski, J. K., Dmitrzak-Weglar, M., Kliwicki, S. & Hauser, J. Polymorphism of circadian clock genes and prophylactic lithium response. *Bipolar Disord.* **16**, 151–158 (2014).

45. Geoffroy, P. A. *et al.* Circadian genes and lithium response in bipolar disorders: associations with PPARGC1A (PGC-1α) and RORA. *Genes Brain Behav.* **15**, 660–668 (2016).

46. Maier, R. M., Visscher, P. M., Robinson, M. R. & Wray, N. R. Embracing polygenicity: a review of methods and tools for psychiatric genetics research. *Psychol. Med.* **48**, 1055–1067 (2018).

47. de Leeuw, C. A., Neale, B. M., Heskes, T. & Posthuma, D. The statistical properties of gene-set analysis. *Nat. Rev. Genet.* **17**, 353–364 (2016).

48. de Leeuw, C. A., Mooij, J. M., Heskes, T. & Posthuma, D. MAGMA: generalized gene-set analysis of GWAS data. *PLoS Comput. Biol.* **11**, e1004219 (2015).

49. Lee, P. H., O'Dushlaine, C., Thomas, B. & Purcell, S. M. INRICH: interval-based enrichment analysis for genome-wide association studies. *Bioinforma. Oxf. Engl.* **28**, 1797–1799 (2012).

50. Zhang, E. E. *et al.* A genome-wide RNAi screen for modifiers of the circadian clock in human cells. *Cell* **139**, 199–210 (2009).

51. Takahashi, J. S. Transcriptional architecture of the mammalian circadian clock. *Nat. Rev. Genet.* **18**, 164–179 (2017).

52. McCarthy, M. J., Nievergelt, C. M., Kelsoe, J. R. & Welsh, D. K. A survey of genomic studies supports association of circadian clock genes with bipolar disorder spectrum illnesses and lithium response. *PloS One* **7**, e32091 (2012).

53. Byrne, E. M. *et al.* Testing the role of circadian genes in conferring risk for psychiatric disorders. *Am. J. Med. Genet. Part B Neuropsychiatr. Genet. Off. Publ. Int. Soc. Psychiatr. Genet.* **165B**, 254–260 (2014).

54. Yan, J., Wang, H., Liu, Y. & Shao, C. Analysis of gene regulatory networks in the mammalian circadian rhythm. *PLoS Comput. Biol.* **4**, e1000193 (2008).

55. Pizarro, A., Hayer, K., Lahens, N. F. & Hogenesch, J. B. CircaDB: a database of mammalian circadian gene expression profiles. *Nucleic Acids Res.* **41**, D1009-1013 (2013).

56. Li, J. Z. *et al.* Circadian patterns of gene expression in the human brain and disruption in major depressive disorder. *Proc. Natl. Acad. Sci.* **110**, 9950–9955 (2013).

57. Chen, C.-Y. *et al.* Effects of aging on circadian patterns of gene expression in the human prefrontal cortex. *Proc. Natl. Acad. Sci. U. S. A.* **113**, 206–211 (2016).

58. Schizophrenia Working Group of the Psychiatric Genomics Consortium. Biological insights from 108 schizophrenia-associated genetic loci. *Nature* **511**, 421–427 (2014).

59. Duncan, L. E. *et al.* Largest GWAS of PTSD (N=20 070) yields genetic overlap with schizophrenia and sex differences in heritability. *Mol. Psychiatry* **23**, 666–673 (2018).

60. Wray, N. R. *et al.* Genome-wide association analyses identify 44 risk variants and refine the genetic architecture of major depression. *Nat. Genet.* **50**, 668–681 (2018).

61. Hou, L. *et al.* Genome-wide association study of 40,000 individuals identifies two novel loci associated with bipolar disorder. *Hum. Mol. Genet.* **25**, 3383–3394 (2016).

62. Grove, J. *et al.* Identification of common genetic risk variants for autism spectrum disorder. *Nat. Genet.* **51**, 431–444 (2019).

63. Demontis, D. *et al.* Discovery of the first genome-wide significant risk loci for attention deficit/hyperactivity disorder. *Nat. Genet.* **51**, 63–75 (2019).

64. Jones, S. E. *et al.* Genome-Wide Association Analyses in 128,266 Individuals Identifies New Morningness and Sleep Duration Loci. *PLoS Genet.* **12**, e1006125 (2016).

65. Hou, L. *et al.* Genetic variants associated with response to lithium treatment in bipolar disorder: a genome-wide association study. *The Lancet* **387**, 1085–1093 (2016).

66. Chang, C. C. *et al.* Second-generation PLINK: rising to the challenge of larger and richer datasets. *GigaScience* **4**, 7 (2015).

67. Watanabe, K., Taskesen, E., van Bochoven, A. & Posthuma, D. Functional mapping and annotation of genetic associations with FUMA. *Nat. Commun.* **8**, 1826 (2017).

68. Manchia, M. *et al.* Assessment of Response to Lithium Maintenance Treatment in Bipolar Disorder: A Consortium on Lithium Genetics (ConLiGen) Report. *PloS One* **8**, e65636 (2013).

69. Schulze, T. G. *et al.* The International Consortium on Lithium Genetics (ConLiGen): an initiative by the NIMH and IGSLI to study the genetic basis of response to lithium treatment. *Neuropsychobiology* **62**, 72–78 (2010).

70. R Core Team. *R: A Language and Environment for Statistical Computing*. (R Foundation for Statistical Computing, 2022).

71. *IBM SPSS Statistics for Windows*. (IBM Corp., 2017).

72. Wickham, H. Introduction. in *ggplot2: Elegant Graphics for Data Analysis* (ed. Wickham, H.) 1–7 (Springer, 2009). doi:10.1007/978-0-387-98141-3_1.

73. Sarkar, D. *Lattice: Multivariate Data Visualization with R*. (Springer, 2008).

74. Hurst, J. L. & West, R. S. Taming anxiety in laboratory mice. *Nat. Methods* **7**, 825–826 (2010).

75. Volkmann, P., Stephan, M., Krackow, S., Jensen, N. & Rossner, M. J. PsyCoP - A Platform for Systematic Semi-Automated Behavioral and Cognitive Profiling Reveals Gene and Environment Dependent Impairments of Tcf4 Transgenic Mice Subjected to Social Defeat. *Front. Behav. Neurosci.* **14**, 618180 (2020).

76. Hühne, A., Volkmann, P., Stephan, M., Rossner, M. & Landgraf, D. An In-Depth Neurobehavioral Characterization Reveals Anxiety-like Traits, Impaired Habituation Behavior, and Restlessness in Male Cryptochrome-deficient Mice. *Genes Brain Behav.* **19**, e12661.

77. Wickham, H. *ggplot2: elegant graphics for data analysis*. (Springer, 2016).

78. Kolde, R. *pheatmap: Pretty Heatmaps*. (2019).

79. Fox, J. & Weisberg, S. *An R Companion to Applied Regression*. (2019).

80. Dray, S. & Dufour, A.-B. The ade4 Package: Implementing the Duality Diagram for Ecologists. *J. Stat. Softw.* **22**, 1–20 (2007).

81. Friendly, M. & Fox, J. *candisc: Visualizing Generalized Canonical Discriminant and Canonical Correlation Analysis*. (2021).

82. Anderzhanova, E., Kirmeier, T. & Wotjak, C. T. Animal models in psychiatric research: The RDoC system as a new framework for endophenotype-oriented translational neuroscience. *Neurobiol. Stress* **7**, 47–56 (2017).

83. Romagnoli, D. *et al.* ddSeeker: a tool for processing Bio-Rad ddSEQ single cell RNA-seq data. *BMC Genomics* **19**, 960 (2018).

84. Dobin, A. *et al.* STAR: ultrafast universal RNA-seq aligner. *Bioinforma. Oxf. Engl.* **29**, 15–21 (2013).

85. Hao, Y. *et al.* Integrated analysis of multimodal single-cell data. *Cell* **184**, 3573-3587.e29 (2021).

86. Hafemeister, C. & Satija, R. Normalization and variance stabilization of single-cell RNA-seq data using regularized negative binomial regression. *Genome Biol.* **20**, 296 (2019).

87. McInnes, L., Healy, J. & Melville, J. UMAP: Uniform Manifold Approximation and Projection for Dimension Reduction. *ArXiv180203426 Cs Stat* (2020).

88. McDavid, A., Finak, G. & Yajima, M. *MAST: Model-based Analysis of Single Cell Transcriptomics*. (2020).

89. Zhou, Y. *et al.* Metascape provides a biologist-oriented resource for the analysis of systems-level datasets. *Nat. Commun.* **10**, 1523 (2019).

90. Koopmans, F. *et al.* SynGO: An Evidence-Based, Expert-Curated Knowledge Base for the Synapse. *Neuron* **103**, 217-234.e4 (2019).

91. Herholt, A. *et al.* Pathway sensor-based functional genomics screening identifies modulators of neuronal activity. *Sci. Rep.* **8**, 17597 (2018).

92. Teng, Z., Zhang, M., Zhao, M. & Zhang, W. Glucocorticoid exerts its non-genomic effect on IPSC by activation of a phospholipase C-dependent pathway in prefrontal cortex of rats. *J. Physiol.* **591**, 3341–3353 (2013).

93. Hu, W., Zhang, M., Czéh, B., Flügge, G. & Zhang, W. Stress Impairs GABAergic Network Function in the Hippocampus by Activating Nongenomic Glucocorticoid Receptors and Affecting the Integrity of the Parvalbumin-Expressing Neuronal Network. *Neuropsychopharmacology* **35**, 1693–1707 (2010).

94. Zhang, M., Weiland, H., Schöfbänker, M. & Zhang, W. Estrogen Receptors Alpha and Beta Mediate Synaptic Transmission in the PFC and Hippocampus of Mice. *Int. J. Mol. Sci.* **22**, 1485 (2021).

95. Wehr, M. C. *et al.* Spironolactone is an antagonist of NRG1-ERBB4 signaling and schizophrenia-relevant endophenotypes in mice. *EMBO Mol. Med.* **9**, 1448–1462 (2017).

96. Saffari, R. *et al.* NPY+-, but not PV+-GABAergic neurons mediated long-range inhibition from infra- to prelimbic cortex. *Transl. Psychiatry* **6**, e736–e736 (2016).

97. Agarwal, A. *et al.* Dysregulated Expression of Neuregulin-1 by Cortical Pyramidal Neurons Disrupts Synaptic Plasticity. *Cell Rep.* **8**, 1130–1145 (2014).

98. Shahmoradi, A., Radyushkin, K. & Rossner, M. J. Enhanced memory consolidation in mice lacking the circadian modulators Sharp1 and -2 caused by elevated Igf2 signaling in the cortex. *Proc. Natl. Acad. Sci. U. S. A.* **112**, E3582–E3589 (2015).

99. Rossner, M. J. *et al.* Disturbed Clockwork Resetting in Sharp-1 and Sharp-2 Single and Double Mutant Mice. *PLoS ONE* **3**, (2008).

100. Lucini-Paioni, S., Squarcina, L., Cousins, D. A. & Brambilla, P. Lithium effects on Hippocampus volumes in patients with bipolar disorder. *J. Affect. Disord.* **294**, 521–526 (2021).

101. Brzózka, M. M., Havemann-Reinecke, U., Wichert, S. P., Falkai, P. & Rossner, M. J. Molecular Signatures of Psychosocial Stress and Cognition Are Modulated by Chronic Lithium Treatment. *Schizophr. Bull.* **42**, S22–S33 (2016).

102. Wang, Y. *et al.* Lithium chloride ameliorates cognition dysfunction induced by sevoflurane anesthesia in rats. *FEBS Open Bio* **10**, 251–258 (2020).

103. King, M. K. & Jope, R. S. Lithium treatment alleviates impaired cognition in a mouse model of fragile X syndrome. *Genes Brain Behav.* **12**, 723–731 (2013).

104. Shim, S. S., Hammonds, M. D., Ganocy, S. J. & Calabrese, J. R. Effects of sub-chronic lithium treatment on synaptic plasticity in the dentate gyrus of rat hippocampal slices. *Prog. Neuropsychopharmacol. Biol. Psychiatry* **31**, 343–347 (2007).

105. Nocjar, C., Hammonds, M. D. & Shim, S. S. Chronic lithium treatment magnifies learning in rats. *Neuroscience* **150**, 774–788 (2007).

106. Twining, R. C., Lepak, K., Kirry, A. J. & Gilmartin, M. R. Ventral Hippocampal Input to the Prelimbic Cortex Dissociates the Context from the Cue Association in Trace Fear Memory. *J. Neurosci. Off. J. Soc. Neurosci.* **40**, 3217–3230 (2020).

107. Avigan, P. D., Cammack, K. & Shapiro, M. L. Flexible spatial learning requires both the dorsal and ventral hippocampus and their functional interactions with the prefrontal cortex. *Hippocampus* **30**, 733–744 (2020).

108. Brown, T. I., Gagnon, S. A. & Wagner, A. D. Stress Disrupts Human Hippocampal-Prefrontal Function during Prospective Spatial Navigation and Hinders Flexible Behavior. *Curr. Biol.* **30**, 1821-1833.e8 (2020).

109. Honma, S. *et al.* Dec1 and Dec2 are regulators of the mammalian molecular clock. *Nature* **419**, 841–844 (2002).

110. Hoover, W. B. & Vertes, R. P. Anatomical analysis of afferent projections to the medial prefrontal cortex in the rat. *Brain Struct. Funct.* **212**, 149–179 (2007).

111. Liu, X. & Carter, A. G. Ventral Hippocampal Inputs Preferentially Drive Corticocortical Neurons in the Infralimbic Prefrontal Cortex. *J. Neurosci.* **38**, 7351–7363 (2018).

112. Rossner, M. J., Dörr, J., Gass, P., Schwab, M. H. & Nave, K.-A. SHARPs: MammalianEnhancer-of-Split- andHairy-Related Proteins Coupled to Neuronal Stimulation. *Mol. Cell. Neurosci.* **9**, 460–475 (1997).

113. Pellegrino, R. *et al.* A Novel BHLHE41 Variant is Associated with Short Sleep and Resistance to Sleep Deprivation in Humans. *Sleep* **37**, 1327–1336 (2014).

114. Orsini, C. A., Kim, J. H., Knapska, E. & Maren, S. Hippocampal and prefrontal projections to the basal amygdala mediate contextual regulation of fear after extinction. *J. Neurosci. Off. J. Soc. Neurosci.* **31**, 17269–17277 (2011).

115. Heroux, N. A., Horgan, C. J., Pinizzotto, C. C., Rosen, J. B. & Stanton, M. E. Medial prefrontal and ventral hippocampal contributions to incidental context learning and memory in adolescent rats. *Neurobiol. Learn. Mem.* **166**, 107091 (2019).

116. Shah, D. & Verhoye, M. Acquisition of Spatial Search Strategies and Reversal Learning in the Morris Water Maze Depend on Disparate Brain Functional Connectivity in Mice. 11.

117. Phillips, R. G. & LeDoux, J. E. Differential contribution of amygdala and hippocampus to cued and contextual fear conditioning. *Behav. Neurosci.* **106**, 274–285 (1992).

118. Bora, E., Fornito, A., Yücel, M. & Pantelis, C. Voxelwise Meta-Analysis of Gray Matter Abnormalities in Bipolar Disorder. *Biol. Psychiatry* **67**, 1097–1105 (2010).

119. Ellison-Wright, I. & Bullmore, E. Anatomy of bipolar disorder and schizophrenia: A meta-analysis. *Schizophr. Res.* **117**, 1–12 (2010).

120. Otten, M. Hippocampal structure and function in individuals with bipolar disorder_ A systematic review. *J. Affect. Disord.* 13 (2015).

121. Hibar, D. P. *et al.* Cortical abnormalities in bipolar disorder: an MRI analysis of 6503 individuals from the ENIGMA Bipolar Disorder Working Group. *Mol. Psychiatry* **23**, 932–942 (2018).

122. Shao, L., Young, L. T. & Wang, J.-F. Chronic treatment with mood stabilizers lithium and valproate prevents excitotoxicity by inhibiting oxidative stress in rat cerebral cortical cells. *Biol. Psychiatry* **58**, 879–884 (2005).

123. Rodríguez-Tornos, F. M., San Aniceto, I., Cubelos, B. & Nieto, M. Enrichment of Conserved Synaptic Activity-Responsive Element in Neuronal Genes Predicts a Coordinated Response of MEF2, CREB and SRF. *PLoS ONE* **8**, e53848 (2013).

124. Kawashima, T. *et al.* Synaptic activity-responsive element in the Arc/Arg3.1 promoter essential for synapse-to-nucleus signaling in activated neurons. *Proc. Natl. Acad. Sci.* **106**, 316–321 (2009).

125. Wu, T.-N. *et al.* Lithium and GADL1 regulate glycogen synthase kinase-3 activity to modulate KCTD12 expression. *Sci. Rep.* **9**, 1–10 (2019).

126. Böer, U. *et al.* Chronic Lithium Salt Treatment Reduces CRE/CREB-Directed Gene Transcription and Reverses Its Upregulation by Chronic Psychosocial Stress in Transgenic Reporter Gene Mice. *Neuropsychopharmacology* **33**, 2407–2415 (2008).

127. Böer, U. *et al.* CRE/CREB-Driven Up-Regulation of Gene Expression by Chronic Social Stress in CRE-Luciferase Transgenic Mice: Reversal by Antidepressant Treatment. *PLoS ONE* **2**, e431 (2007).

128. Lonze, B. E. & Ginty, D. D. Function and Regulation of CREB Family Transcription Factors in the Nervous System. *Neuron* **35**, 605–623 (2002).

129. Steven, A. *et al.* What turns CREB on? And off? And why does it matter? *Cell. Mol. Life Sci.* **77**, 4049–4067 (2020).

130. Quiroz, J. A., Gould, T. D. & Manji, H. K. Molecular effects of lithium. *Mol. Interv.* **4**, 259–272 (2004).

131. Wei, H., Landgraf, D., Wang, G. & McCarthy, M. J. Inositol polyphosphates contribute to cellular circadian rhythms: Implications for understanding lithium's molecular mechanism. *Cell. Signal.* **44**, 82–91 (2018).

132. Tobe, B. T. D. *et al.* Probing the lithium-response pathway in hiPSCs implicates the phosphoregulatory set-point for a cytoskeletal modulator in bipolar pathogenesis. *Proc. Natl. Acad. Sci.* **114**, E4462–E4471 (2017).

133. Sakamoto, K., Karelina, K. & Obrietan, K. CREB: a multifaceted regulator of neuronal plasticity and protection. *J. Neurochem.* **116**, 1–9 (2011).

Paper VI – Supplementary Figures

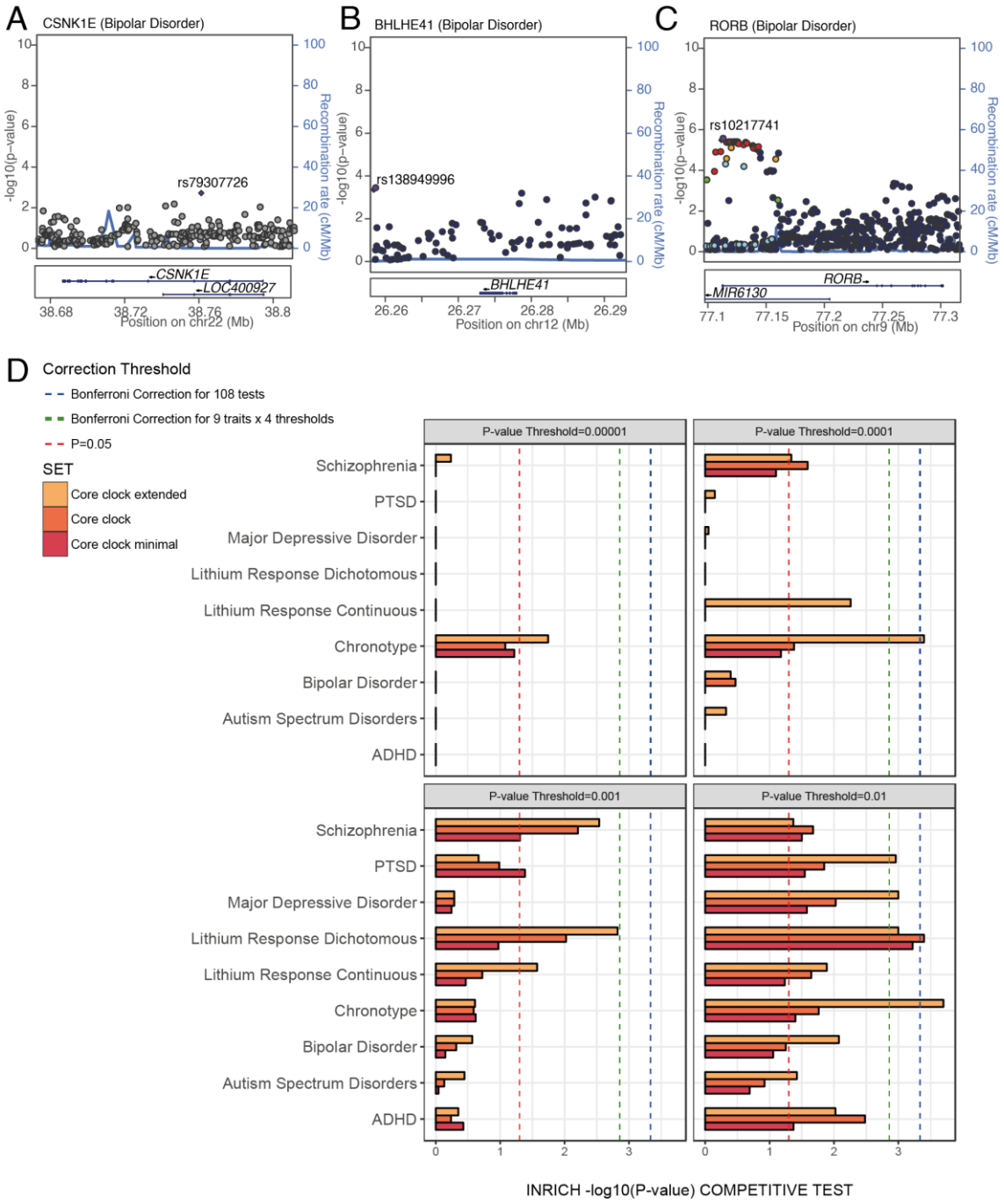

Figure S1. BD risk Manhattan plots & INRICH analyses based on core clock gene-sets in psychiatric traits. (A - C) Regional Manhattan plots for BD risk of the top three genes in the core clock gene-set (15 KB up-and downstream of the respective gene). (D) Competitive test P-values in the X-axis are –log10 converted. Four different P-value thresholds were analyzed (P = 0.00001, P = 0.0001, P = 0.001, P = 0.01). Bonferroni significance thresholds: dashed blue line (P < 0.05/ (3 gene-sets x 9 traits x 4 thresholds)); dashed green line indicates a less stringent Bonferroni significance threshold (P < 0.05/ (9 traits x 4 thresholds)). Dashed red line indicates the nominal (uncorrected) significance threshold P = 0.05. ADHD: Attention-Deficit/Hyperactivity Disorder; PTSD: Post-Traumatic Stress Disorder.

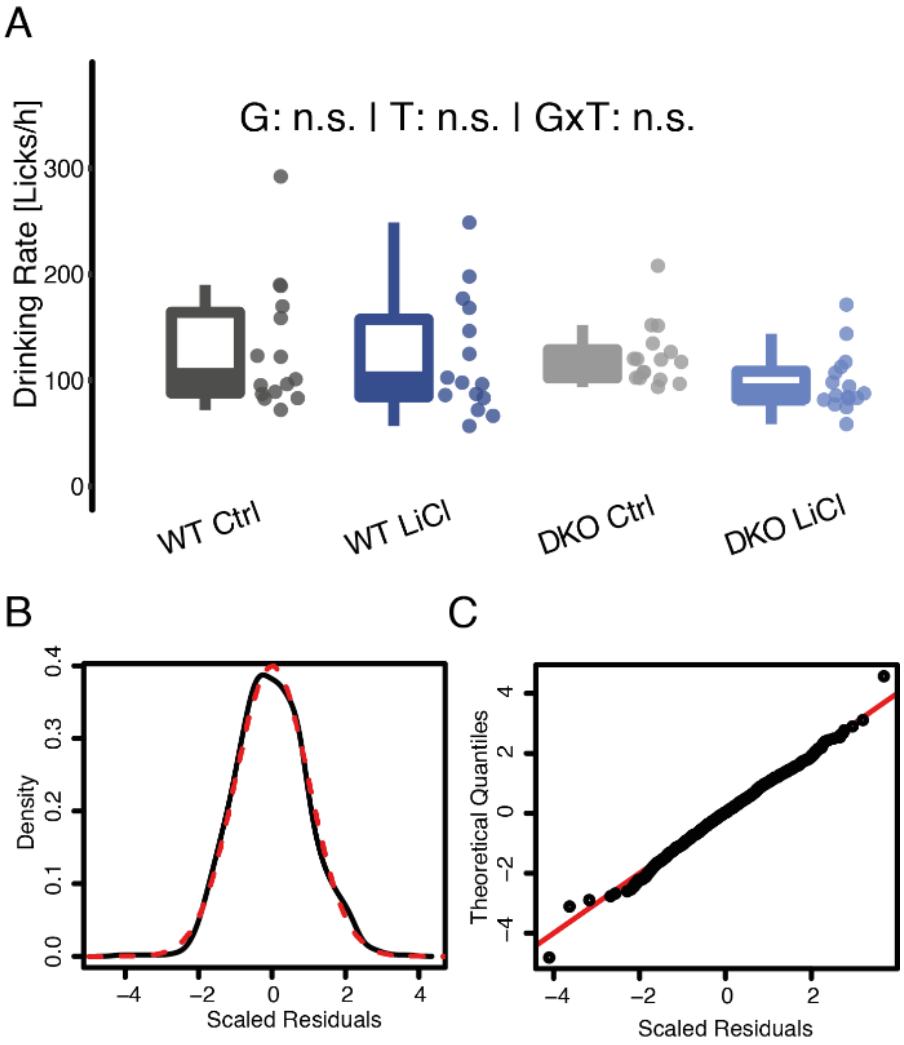

Figure S2. Quality controls for the PsyCoP behavioral study. (A) Drinking rate in the IntelliCage during the experiments was not significantly different in lithium chloride-treated mice compared to control. Data are shown as box plots with whiskers extending to no more than 1.5-fold IQR. (B) Density plot and QQ plot of the scaled residuals (black) of the multivariate linear model used for the ANOVA procedure of all PsyCoP measures compared to a normal distribution (red) show no major deviations. * $P < 0.05$, ** $P < 0.01$, *** $P < 0.001$, n.s. not significant; P-values are FDR-adjusted and refer to Wilk's lambda testing two-way ANOVA; G: genotype term; T: lithium treatment term; GxT: interaction term; WT: wildtype; DKO: Bhlhe40/41 double-knockout; Ctrl: vehicle control; LiCl: lithium-treated

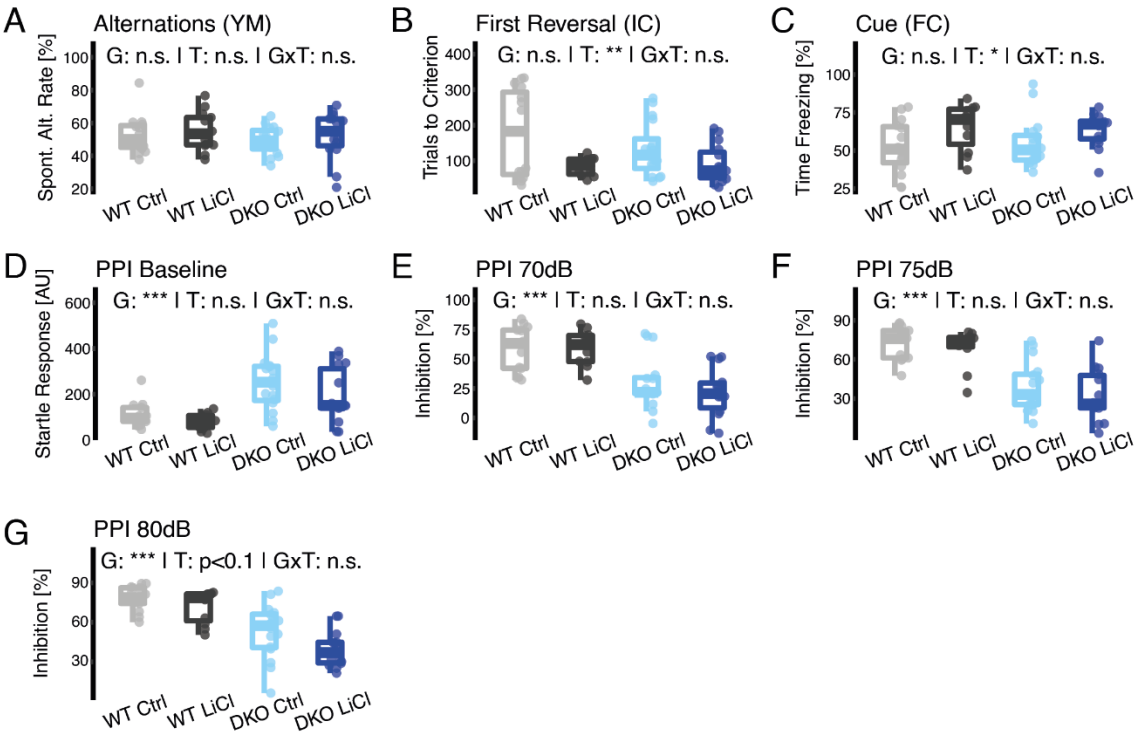

Figure S3. Remaining variables of the cognition and sensorimotor RDoC domains. (A-C) display the variables of the Cognitive RDoC domain not shown in Figure 2. (A) There was no significant effect on working memory in the Y-Maze test measured with the rate of spontaneous alternations between arms. (B) In the first reversal lithium treated mice needed less trials to reach the learning criterion indicating improved learning flexibility. Although, the difference in Bhlhe40/41 DKO mice was smaller than in wildtypes, the interaction was not significant in this part of the spatial learning experiments. (C) Similarly, in the cued fear memory task, lithium treatment increased the time spent freezing, showing improved cued fear memory, with no significant influence of the Bhlhe40/41 double-knockout. (D-G) show the variables of the Sensorimotor domain with a strong genotype effect in all of them, but only minor influence of lithium treatment on the highest prepulse level (PPI 80dB) in panel (G). Data are shown as box plots with whiskers extending to no more than 1.5-fold IQR; * P < 0.05, ** P < 0.01, *** P < 0.001, n.s. not significant; P-values are FDR-adjusted and refer to Wilk's lambda testing two-way ANOVA; G: genotype term; T: lithium treatment term; GxT: interaction term; WT: wildtype; DKO: Bhlhe40/41 double-knockout; Ctrl: Placebo control; LiCl: lithium-treated

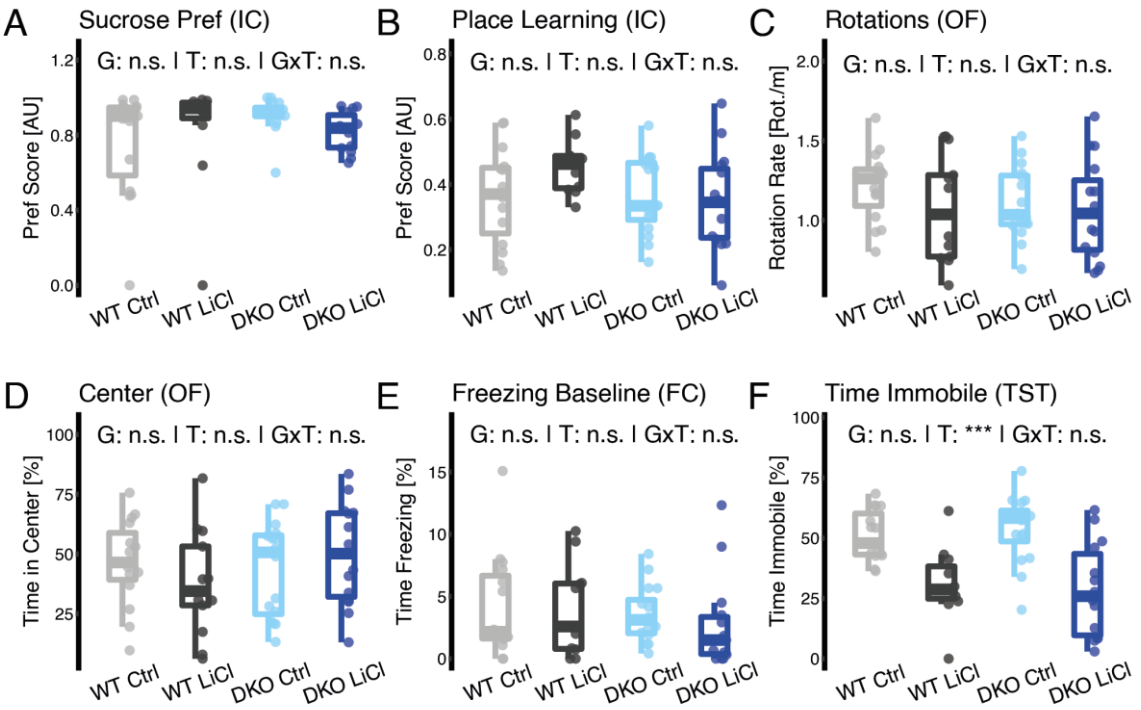

Figure S4. Positive and Negative Valence RDoC domains. The variables associated with positive valence systems did show significant effects neither in the Sucrose Preference Test (A) nor the place preference in Positive Reinforcement Learning (B). Notably, there was a sex difference in sucrose preference detected, shown in Figure S6. In the negative valence domain parameters, there were no significant differences in rotation rate (C) and the center time (D) in the Open Field Test as well as the baseline freezing behavior (E) in Fear Conditioning. However, lithium-treated mice were significantly less immobile (F) in the Tail Suspension Test, independent of genotype. Data are shown as box plots with whiskers extending to no more than 1.5-fold IQR; * P < 0.05, ** P < 0.01, *** P < 0.001, n.s. not significant; P-values are FDR-adjusted and refer to Wilk's lambda testing two-way ANOVA; G: genotype term; T: lithium treatment term; GxT: interaction term; WT: wildtype; DKO: Bhlhe40/41 double-knockout; Ctrl: Placebo control; LiCl: lithium-treated

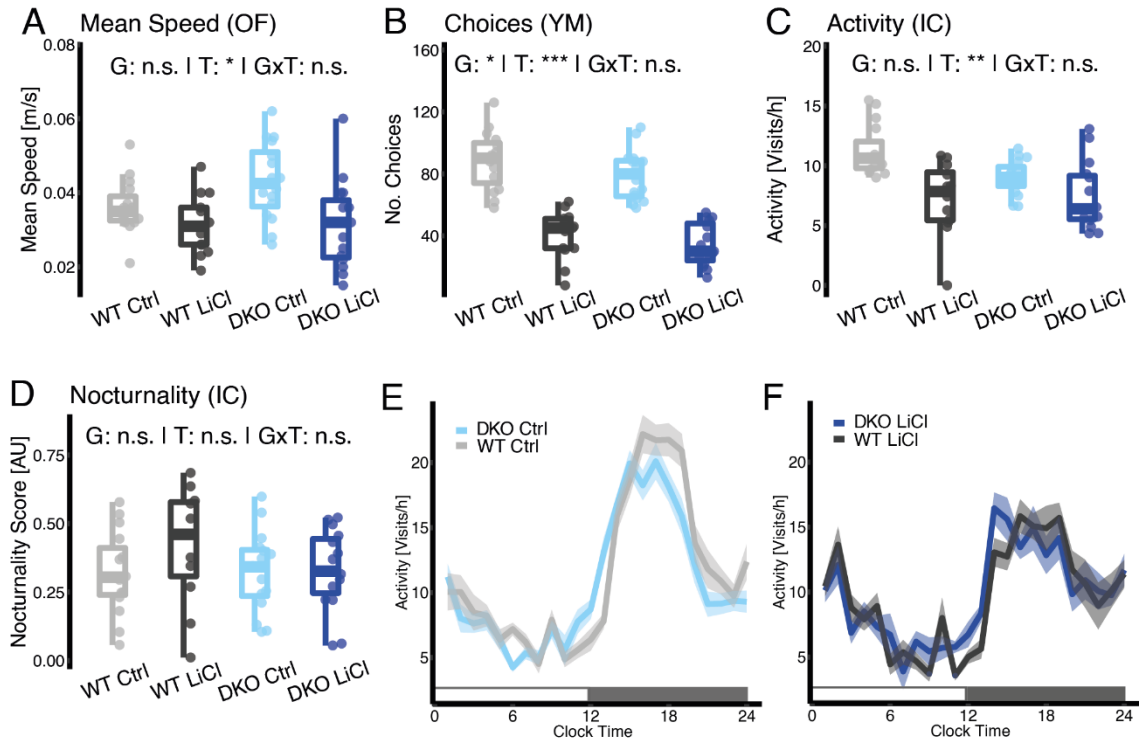

Figure S5. Arousal and Regulatory RDoC domain. Novelty-induced activity was reduced in lithium-treated animals (A) measured as Mean Speed in the Open Field Test and (B) the number of arm choices in the Y-Maze Test. In latter case Bhlhe40/41 DKO mice displayed a slightly reduced activity, as well, independent

of treatment. General Activity (C) in the IntelliCage was similarly reduced in response to lithium treatment. Please note that there was a sex difference in activity level in response to lithium treatment shown in Figure S6 with males being impacted stronger than females. There was no significant difference in preference for nighttime activity versus daytime activity measured as nocturnality score (D). We could not detect a significant effect of the Bhlhe40/41 double-knockout on the distribution of activity over daytime, neither control (E) nor lithium-treated (F) mice. (A-D) Data are shown as box plots with whiskers extending to no more than 1.5-fold IQR; * P < 0.05, ** P < 0.01, *** P < 0.001, n.s. not significant; P-values are FDR-adjusted and refer to Wilk's lambda testing two-way ANOVA; (E-F) Lines represent group means of 1-hour bins and ribbons show the standard error of the mean. The light and dark bars visualize the light and dark phase, respectively. G: genotype term; T: lithium treatment term; GxT: interaction term; WT: wildtype; DKO: Bhlhe40/41 double-knockout; Ctrl: Placebo control; LiCl: lithium-treated

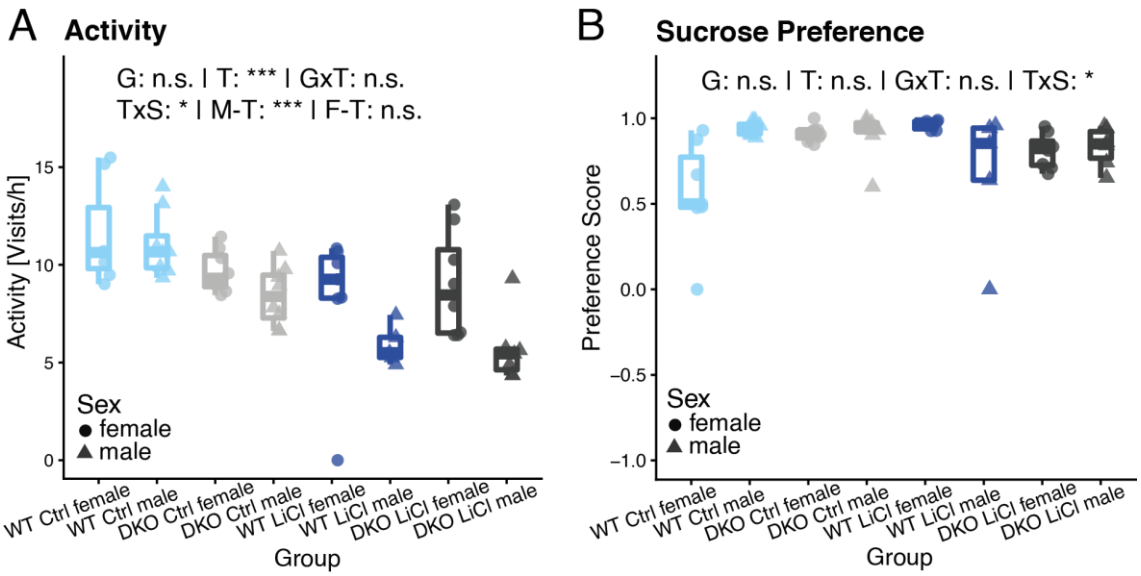

Figure S6. Sex Differences in general activity and sucrose preference. In most behavioral parameters assessed we did not detect significant differences between sexes (Table S3). (A) However, male mice showed a stronger reduction in general activity in response to lithium treatment than female mice. (B) Moreover, the female wildtype placebo control (WT Ctrl female) group displayed a lower sucrose preference than their lithium-treated counterpart. This difference in lithium response between sexes was not found in Bhlhe40/41 double-knockout (DKO) mice, which might indicate a methodological artifact, since the groups were housed in separate cages. Data are shown as box plots with whiskers extending to no more than 1.5-fold IQR; * P < 0.05, ** P < 0.01, *** P < 0.001, n.s. not significant; P-values are FDR-adjusted and refer to Wilk's lambda testing two-way ANOVA; n = ; G: genotype term; T: lithium treatment term; GxT: G by T interaction term; TxS: T by sex interaction term; M-T: male treatment effect; F-T: female treatment effect; WT: wildtype; DKO: Bhlhe40/41 double-knockout; Ctrl: Placebo control; LiCl: lithium-treated

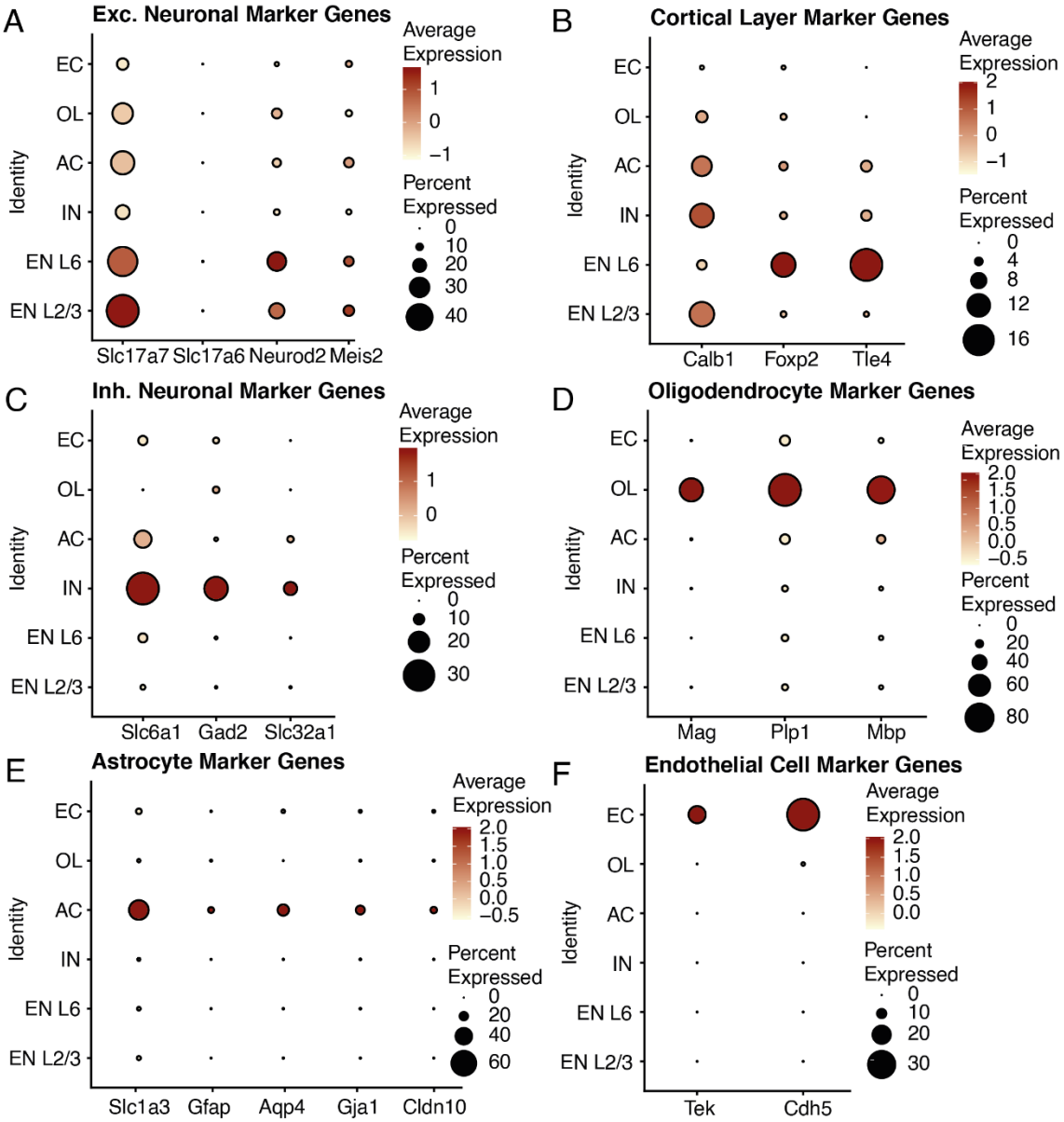

Figure S7. Dot plots of selected cluster marker genes. Normalized average expression is shown in color scale, abundance of expressing cells in percent as dot size. (A) Excitatory neuron marker genes are highly enriched in both excitatory neuron (EN) clusters (EN L2/3 and EN L6). However, those genes are not exclusively expressed in those clusters. For example, Slc17a7 (Solute carrier family 17 member 7; VGLUT1) is expressed in astrocytes (AC) and oligodendroglial cells (OL). (B) Similarly, the expression of Calb1 (Calbindin 1) in ENs indicates an upper layer identity, while not being exclusively expressed in ENs. Thus, it serves as a cortical layer 2/3 marker (EN L2/3), whereas Foxp2 (Forkhead-Box-Protein P2) and Tle4 (Transducin-like enhancer protein 4) are highly expressed in layer 6 principal neurons (EN L6). (C) Inhibitory neurons are marked out by the expression of GABA transporters and synthesis enzymes. (D) Oligodendrocytes are identified with the help of myelin-associated genes, (E) astrocytes with a variety of markers for subpopulations, especially reactive astrocytes. (F) Endothelial cells (EC), on the other hand, have a very distinct transcriptional profile with Tek (TEK receptor tyrosine kinase) and Cdh5 (Cadherin 5) as an example.

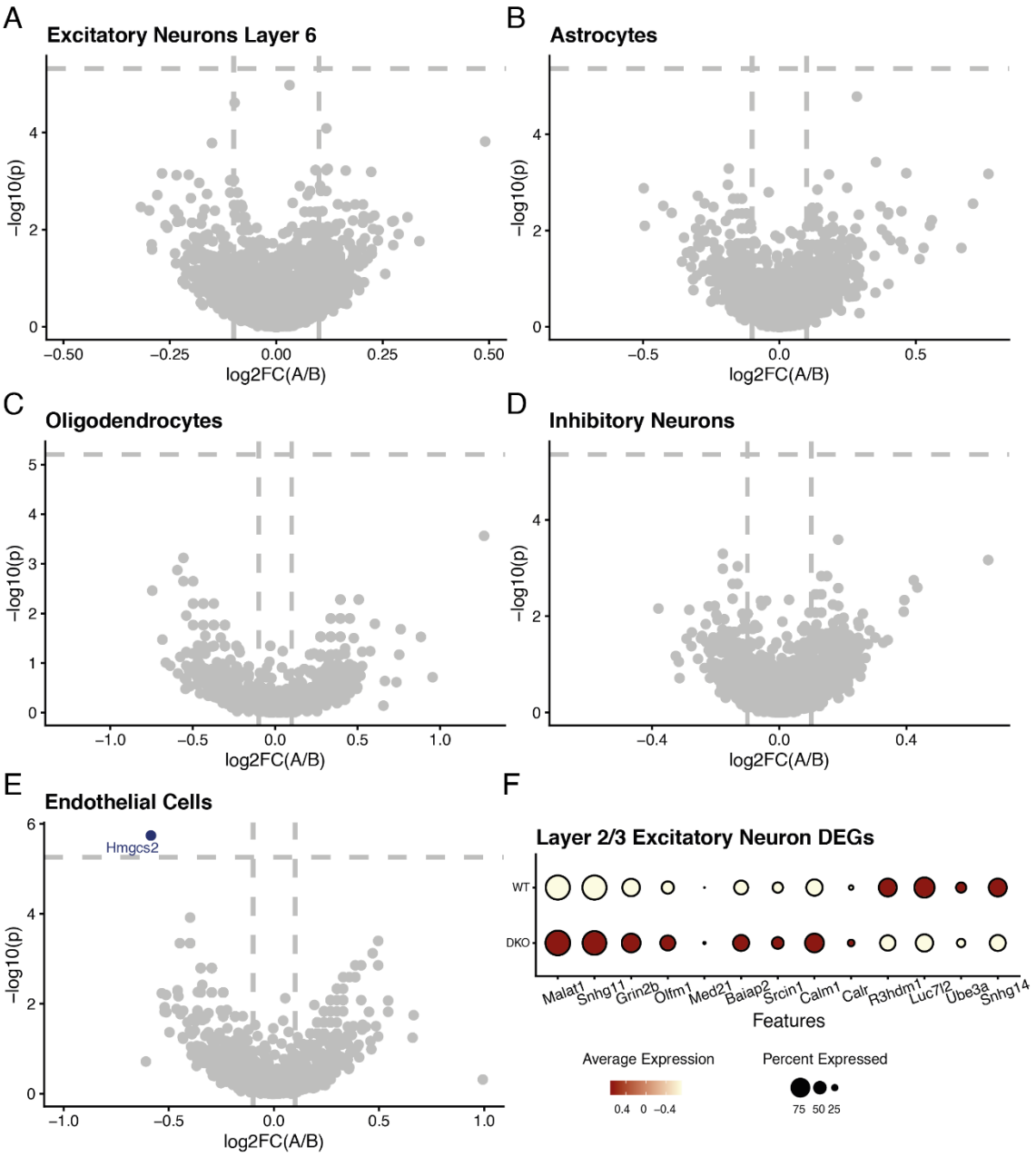

Figure S8. Volcano plots of the differential expression analysis for all remaining clusters. (A-D) The differential expression analysis between Bhlhe40/41 double-knockout (DKO) and wildtype (WT) cells in the clusters of layer 6 excitatory neurons (A), inhibitory neurons (B), astrocytes (C) and oligodendocytes (D) did show no significantly differentially expressed genes. In endothelial cells (E) only Hmgcs2 was expressed significantly lower in DKO cells compared to WT. On the Y-axis the unadjusted P-value of the respective MAST analysis is shown with the Šidak-corrected significance level as threshold. The average log2-transformed fold-change is plotted on the X-axis with a threshold of 0.1 for differentially expressed genes. (F) A dot plot of the differentially expressed genes demonstrates that the number of expressing cells is mostly similar between DKO and WT cells, while expression levels are different. Normalized average expression is shown in color scale, abundance of expressing cells in percent as size.

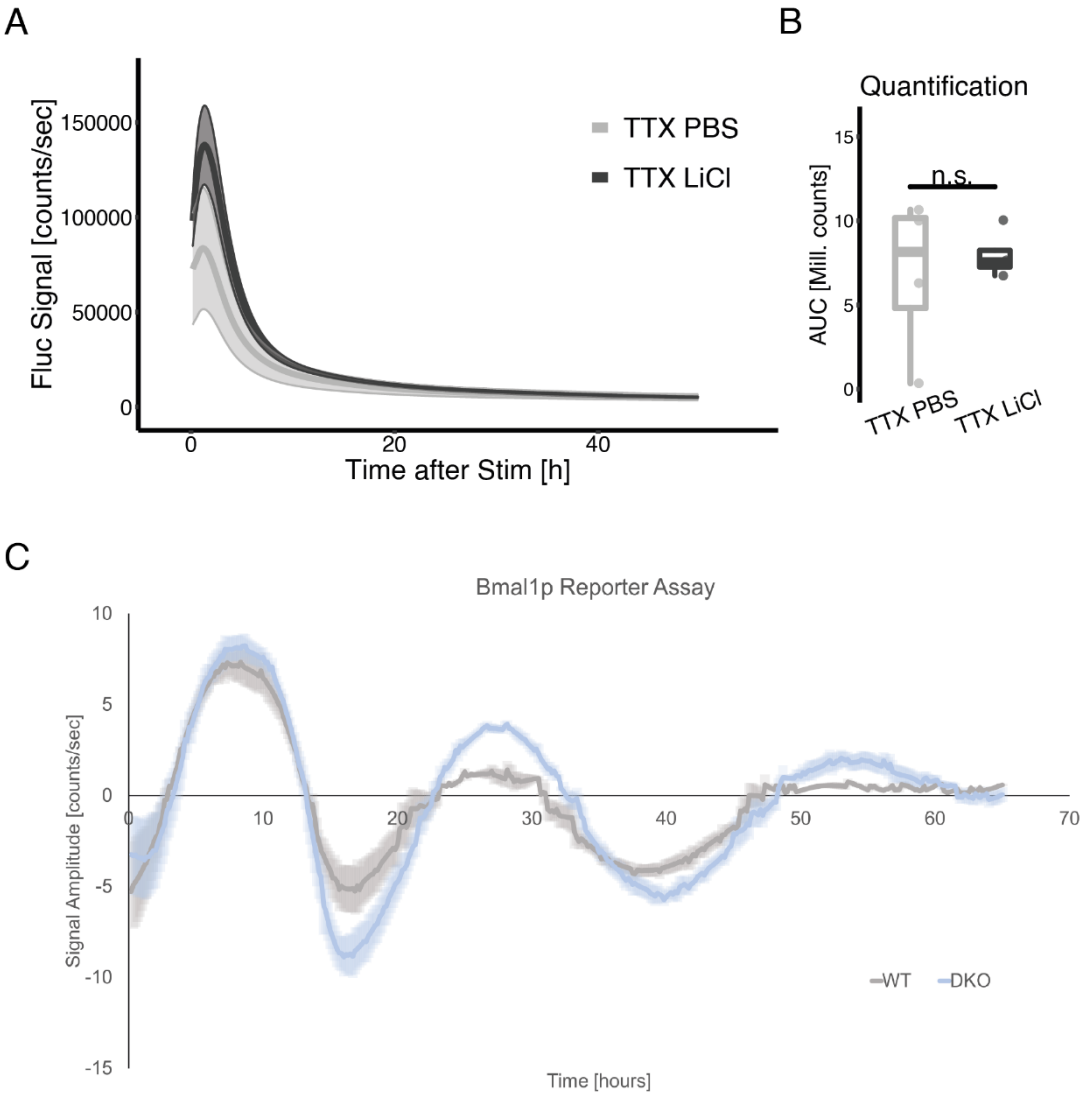

Figure S9. Lithium toxicity test and Bmal1 promoter reporter assay. (A) First 50 hours of tetrodotoxin (TTX)- and AP-V-silenced primary cortical neuron culture from wildtype (WT) embryos after lithium treatment. Cells were transduced with an ESARE-Flirefly Luciferase (Fluc) reporter construct via AAV infection. After 7 days of pretreatment with lithium chloride (LiCl), cultures were treated with a TTX/AP-V cocktail to silence all neuronal network activity. At the start of the recording a typical artifact peak resulting from the time-lag of the transcriptional-translational reporter system, was seen. (B) The area under the curve of the first 100 hours of recording was quantified. No statistically significant difference was found in a Student's two-sided t-test, indicating that differences in ESARE-response are due to activity dampening not cytotoxic effects of lithium chloride. (C) Bmal1 promoter (Bmal1p) reporter assay from cortical neuron cultures of wildtype (WT) and Bhlhe40/41 double-knockout (DKO) mice, respectively. Cells were transduced with a lentiviral reporter construct and, after one week, synchronized with 2µM forskolin. Shown is the mean signal of four replicates with the SEM as ribbon in the background. This assay demonstrates that DKO cortical neurons in culture are still rhythmic and do not display a dampened Bmal1p activity amplitude. n.s.: not significant.

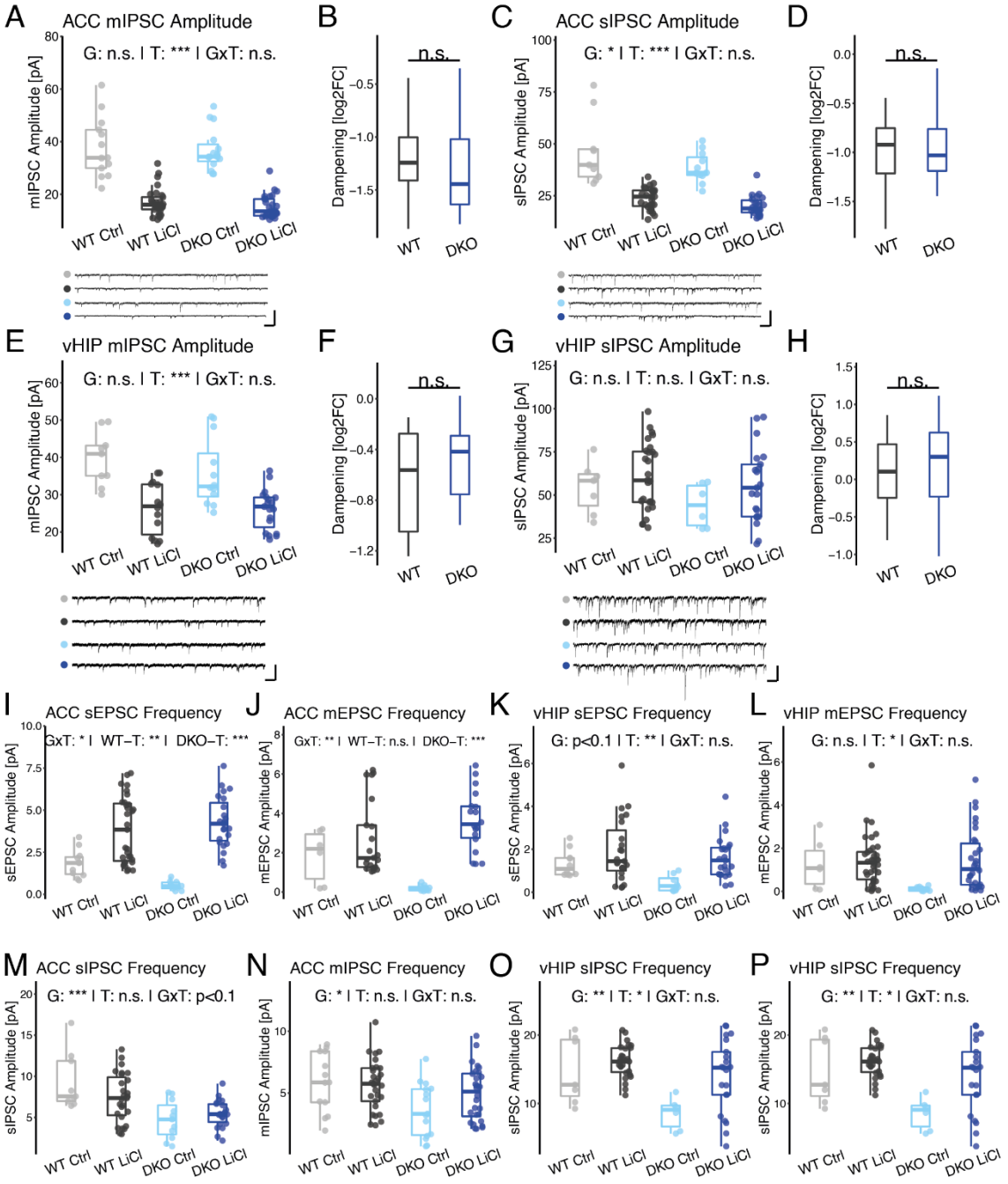

Figure S10. Extended data from whole-cell recordings in ACC and vHIP. Whole-cell voltage-clamp recordings in layer 2/3 pyramidal cells in the anterior cingulate cortex (ACC) area of the medial prefrontal cortex (mPFC) and pyramidal cells in the CA1 region of the ventral hippocampus (vHIP). (A-H) Average miniature and spontaneous inhibitory post-synaptic potential (mIPSC & sIPSC) amplitudes with example traces (scale bars x: 0.2 s & y: 0.1 nA) and the log2-transformed fold change of the respective amplitudes in LiCl compared to Ctrl mice. (I-L) Average miniature and spontaneous excitatory post-synaptic potential (mEPSC & sEPSC) frequency. (M-P) Average mIPSC and sIPSC frequency measured in ACC and vHIP. * P < 0.05; ** P < 0.01; *** P < 0.001; n.s. not significant; P-values refer to univariate two-way ANOVA with Type 2 sum-of-squares; simple effects were tested in a similar but unifactorial ANOVA procedure; WT: wildtype mice; DKO: Bhlhe40/41 double-knockout mice; Ctrl: vehicle control; LiCl: lithium-treated; G: genotype main effect; T: treatment main effect; GxT: interaction effect; simple T: simple effects; DKO-T: DKO simple treatment effect; WT-T: WT simple treatment effect.

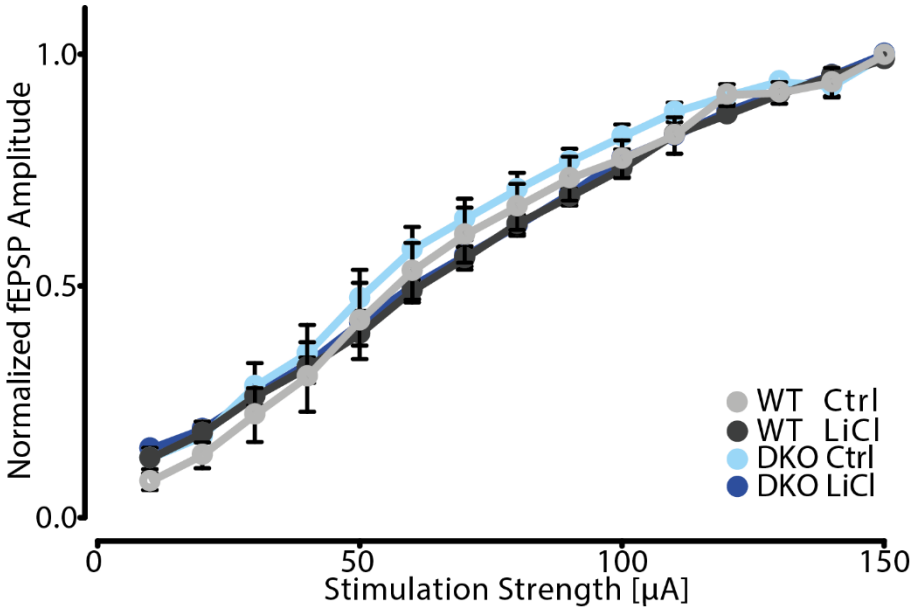

Figure S11. Extended Data on LTP Recordings in the CA1 Region of the Hippocampus. Input output (I/O) relationship of the mean (+/-SEM) normalized field excitatory post-synaptic potential (fEPSP) measured in the CA1 region plotted against the stimulation current injected at the Schaffer collaterals in the stratum radiatum at the CA3/CA1 junction did not show any differences in basic synaptic transmission between groups WT: wildtype mice; DKO: Bhlhe40/41 double-knockout mice; Ctrl: vehicle control; LiCl: lithium-treated

Anhang E: Paper VII

Titel: Expression of Lineage Transcription Factors Identifies Differences in Transition States of Induced Human Oligodendrocyte Differentiation

DOI-Direktlink: https://doi.org/10.3390/cells11020241

Danksagung

An dieser Stelle möchte ich allen Menschen danken, die mich bei all den Projekten und der Anfertigung meiner Dissertation unterstützt haben.

Mein besonderer Dank gilt meinem Doktorvater Moritz Roßner für die ausgezeichnete Betreuung und die enorme Unterstützung nicht nur im Rahmen der Doktorarbeit, sondern auch bei vielen Problemen und Fragen zu meinem akademischen und beruflichen Werdegang. Ich habe mich immer gut unterstützt und wertgeschätzt gefühlt.

Außerdem möchte ich mich bei den Mitgliedern meines *Thesis Advisory Committee,* Carsten Wotjak, Michael Ziller, Sergi Papiol und Dominic Landgraf bedanken, die mich auf meinem Weg immer mit Rat und Anregungen unterstützt haben. Besonderer Dank gilt hier meinem Zweitprüfer Carsten Wotjak, insbesondere auch für seinen Rat und ein offenes Ohr, und Sergi Papiol, der für das Lithium- und das Oligodendrozyten-Projekt Großes geleistet hat und immer geduldig und hilfsbereit auf meine vielen Bitten eingegangen ist.

Auch möchte ich Niels Jensen, Wilma Vogel und Jessica Bly meinen Dank aussprechen, die mich bei allen Experimenten mit Mäusen, begleitet, beraten und tatkräftig unterstützt haben.

Des Weiteren gilt mein Dank auch den Doktoranden und Masterstudenten, die mit mir an vielen der Projekte meiner Doktorarbeit zusammengearbeitet haben oder mich an ihrem Projekt haben teilhaben lassen. Namentlich danken möchte ich an dieser Stelle nennen: Paul Volkmann, Jonathan Schoeller, Anisja Hühne, Florian Raabe, Pia Pickelmann, Philipp Schuler, Elisabeth Voggenreiter, Celestine Dutta, Muriel Frisch, Charlotte Kling und Lisa Echtler.

Ich danke auch ganz besonders Sven Wichert, CEO der *Systasy Bioscience GmbH*, für die fortgesetzte finanzielle Unterstützung, aber auch für Rat und Hilfe bei ungezählten Problemen und natürlich besonders auch für die Einblicke in das Unternehmen sowie die Chance zur Mithilfe und Weiterentwicklung.

Für die organisatorische und finanzielle Unterstützung meiner Weiterbildung möchte ich an dieser Stelle der *International Max Planck Research School for Translational Psychiatry* und ihren Koordinatoren danken.

Nicht zuletzt danke ich all meinen Mitarbeitern, die ich nicht allesamt namentlich erwähnen konnte, die mich aber an vielen Stellen unterstützt haben, und so diese Dissertation erst möglich gemacht haben.

Meinen Eltern, Geschwistern und Freunden danke ich für ihre Ermutigungen während der Doktorarbeit.

Mein besonderer Dank gilt selbstverständlich auch meiner Partnerin, die mich mit mehr Verständnis, Geduld und Einsatz durch die Arbeit an dieser Dissertation gebracht hat, als ich für menschenmöglich gehalten hätte. Du warst und bist mir unersetzlich.